[AMERICAN JOURNAL OF SCIENCE, VOL. 289, FEBRUARY, 1989, P. 105–166]

American Journal of Science

FEBRUARY 1989

A HYDROGEOLOGIC MODEL FOR THE FORMATION OF THE GIANT OIL SANDS DEPOSITS OF THE WESTERN CANADA SEDIMENTARY BASIN

GRANT GARVEN
Department of Earth and Planetary Sciences,
The Johns Hopkins University, Baltimore, Maryland 21218

> *"It would seem to be unnecessary to argue for the widespread movement of underground waters under the influence of gravity and differences of head, yet petroleum geologists, as a rule, appear to have ignored this movement. The well-known facts of artesian circulation through distances of hundreds of miles admit of no dispute"* (J.L. Rich, 1921).

ABSTRACT. This paper investigates the role of regional groundwater flow in the formation of the Alberta heavy oil deposits, a supergiant oil field containing over 4×10^{11} m^3 (2700 billion barrels) of bitumen in Upper Devonian carbonates and Lower Cretaceous sands near the eastern margin of the Western Canada sedimentary basin. A primary agent in the origin of the oil deposits was the presence of a gravity-driven groundwater flow system that operated throughout Tertiary time as a result of foreland basin uplift. Mathematical models of the basin suggest that fluid flow was highly focused by the Upper Devonian carbonate aquifer which acted as a major conduit for both long-distance miscible and immiscible oil migration. Gravity-driven flow and the carbonate aquifer provided the key mechanism for leaching large volumes of source rock in the Mississippian to Cretaceous section of the foreland wedge and in impelling separate-phase oil which migrated into the aquifer from underlying Devonian beds. The associated effect of groundwater flow on forced heat convection allowed for lateral transport of fluids in the aquifer at temperatures around 100°C, with rapid cooling at the discharge end of the flow system. Numerical simulations of soluble- and separate-phase migration, demonstrate that over 80 percent of the giant oil deposit probably accumulated during soluble transport of hydrocarbons. Mass balance calculations require oil concentrations on the order of 1 to 10 ppm for flow periods of 10 to 50 million years. Transport of large volumes of oil waned in later Tertiary time, followed by biodegradation and dissolution of the deposit, as the regional flow was dissipated by further erosion of the landscape.

SYMBOL NOTATION

Roman

a_n	—geometric coefficient in basis function.
A_{nm}	—hydraulic conductance matrix.

b_n —geometric coefficient in basis function.
B_n —buoyancy vector in finite element equation.
c_n —geometric coefficient in basis function.
c_s —specific heat capacity of solid.
c_w —specific heat capacity of water.
C_o —oil concentration in groundwater.
C_B —bulk heat capacity of porous medium.
d —abbreviation for darcy permeability unit.
D_{nm} —hydraulic storage capacity matrix.
$\mathbf{D}$ —mass dispersion coefficient for porous media.
$\mathbf{E}$ —thermal conduction-dispersion coefficient.
$\mathbf{E}_o$ —driving force per unit mass of oil.
$\mathbf{E}_w$ —driving force per unit mass of water.
F_n —lateral heat flux vector.
$\mathbf{F}$ —oil mass flux.
g —gravitational constant.
$\mathbf{g}$ —gravity force per unit mass.
h_m —hydraulic head at node m in mesh.
h_o —petroleum head at the reference state.
h_w —hydraulic head at the reference state.
$\mathbf{J}$ —geothermal heat flux.
J_B —geothermal heat flow at basement unconformity.
J_n —heat flow at node n.
k —superscript denoting current time-step level.
$\mathbf{k}$ —intrinsic permeability tensor.
$\mathbf{K}$ —hydraulic conductivity tensor.
$\mathbf{K}_o$ —effective petroleum conductivity.
$\mathbf{K}_w$ —effective hydraulic conductivity.
m, n —subscripts denoting nodes in mesh.
m_o —total mass of oil.
$\mathbf{n}$ —outward pointing, unit vector normal to boundary.
N —number of nodes in finite element mesh.
o —subscript denoting oil phase component.
p —subscript denoting p-th tracking particle.
p —total fluid pressure.
P_e —Peclet number for convective heat flow.
$\mathbf{q}_o$ —Darcy velocity of oil.
$\mathbf{q}_w$ —Darcy velocity of groundwater.
Q_n —lateral hydraulic flux for node n.
r —subscript denoting r-th reaction.
$\mathbf{r}$ —unit vector tangent to boundary.
R_r —rate of r-th biochemical reaction.
R^e —region associated with element.
R_{nm} —thermal conductance matrix.
$\mathcal{R}$ —uniform random number in the range (0, 1).
s —subscript denoting solid phase.
S_o —fractional saturation of oil for multiphase flow.

S_w —fractional saturation of water for multiphase flow.
S_s —specific storage coefficient of porous medium.
S_{nm} —stream function conductance matrix.
t —time.
T —bulk temperature of porous medium.
T_m —temperature at node m.
T_o —temperature at water table surface.
U_{nm} —thermal storage capacity matrix.
v_o —average linear velocity of oil.
v_w —average linear velocity of water.
w —subscript denoting water phase.
x, z —Cartesian coordinates.
x_p, z_p —particle coordinates.
Z —elevation head above reference datum.

Greek

α —elastic compressibility of porous medium.
α_L —logitudinal dispersivity of porous medium.
α_T —transverse dispersivity of porous medium.
β —compressibility of water at constant temperature.
Γ_o —rate of oil generation per unit volume.
Γ_w —rate of water generation per unit volume.
Δ —area of finite element.
Δt —time step increment in numerical algorithms.
Θ —time step weight factor.
λ —effective thermal conductivity of porous media.
μ —dynamic viscosity of fluid.
μ_o —viscosity of oil.
μ_w —viscosity of water.
μ_{ro} —relative viscosity of oil, μ/μ_o.
μ_{rw} —relative viscosity of water, μ/μ_w.
ν_{or} —stoichiometric coefficient.
ξ —finite element basis function.
ρ —fluid density at reference state.
ρ_o —density of oil.
ρ_w —density of water.
ρ_s —density of solids.
ρ_{ro} —relative oil density, $(\rho_o - \rho)/\rho_o$.
ρ_{rw} —relative water density, $(\rho_w - \rho)/\rho_w$.
σ_o —proportionality constant for oil, K_o/g.
σ_ω —proportionality constant for water, K_ω/g.
Σ —arithmetic summation symbol.
ϕ —effective porosity, intergranular and fracture.
Φ —interpolation function in finite element equations.
Ψ —stream function for groundwater.
Ψ_m —stream function at node m.

ω —salinity of groundwater, as weight percent NaCl.
Ω_e —boundary associated with finite element.

Mathematical

∇ — gradient operator: $\left(\frac{\partial}{\partial_x}, \frac{\partial}{\partial_z}\right)$.

INTRODUCTION

The concept is well established and documented in modern textbooks on petroleum geology (for example, Tissot and Welte, 1978; Hunt, 1979) that most petroleum originates in fine-grained sediments through thermal diagenesis of organic matter followed by primary migration into carrier beds (or aquifers) and secondary migration to reservoir traps. Geochemical and thermal aspects of petroleum generation and alteration are well understood, although the mechanics of oil migration and accumulation in sedimentary basins remain controversial (Magara, 1980, 1986). The primary migration of hydrocarbons through source rocks is thought to occur as separate-phase flow. However, it is the regional movement during secondary migration that provides the key transport mechanism required to accumulate hydrocarbons from dispersed points of origin and focus them into suitable trap environments (Levorsen, 1967). Depending on geochemical conditions, the process of secondary migration could involve the transport of hydrocarbons as immiscible droplets or stringers, as miscible mass in solution, or a combination of both. The forces of buoyancy and capillarity play an additional role in the case of immiscible separate-phase flow.

The concept of long-distance oil migration is applicable to numerous sedimentary basins around the world, especially with respect to giant fields (Demaison, 1977). Geochemical correlations have verified long-distance migration as a prevalent process in intracratonic basins such as the Williston basin (Dow, 1974), the Western Canada basin (Deroo and others, 1977), the Denver basin (Clayton and Swetland, 1980), and the Illinois basin (Stueber, Pushkar, and Hetherington, 1987), to name a few North American examples. Little is known, however, about the regional-scale mechanics of oil migration and its relation to the tectonic and hydrogeologic evolution of the sedimentary basins.

Hydrogeologic modeling is presented in this paper to investigate the role of large-scale regional groundwater flow in the genesis of one of the world's largest accumulation of hydrocarbons, the Alberta oil sands deposits of the Western Canada sedimentary basin. The hydrogeologic modeling entails the formulation of two-dimensional mathematical models capable of predicting fluid flow, heat flow, and mass transport for groundwater and petroleum in a compacted and tectonically stable foreland basin. Numerical simulations of the paleohydrology of western Canada are constructed to test competing hypotheses of miscible, soluble transport and immiscible, separate-phase migration. In both models, regional groundwater flow is assumed to be driven by the topographic relief created from late Tertiary thrusting and uplift in the Rocky Mountain foreland. The hydrologic calculations are also used to infer probable stages in fluid migration and petroleum accumulation during foreland basin evolution.

HYDRAULIC THEORIES ON THE ORIGIN OF OIL

The importance of groundwater flow in petroleum deposit formation has been recognized since Munn (1909) proposed the hydraulic theory of oil and gas accumulation, which was advocated in the geologic literature into the 1930's, most notably by Rich (1921, 1931). According to the theory, disseminated hydrocarbons are focused into carrier beds or aquifers by circulating groundwater. Entrapment of oil and gas occurs at positions where the resistance caused by buoyancy and capillarity forces exceed the transport force of the impelling groundwater. Hubbert (1953) quantified the physical relationship between groundwater movement and petroleum entrapment and showed the ability of petroleum-water interfaces to be tilted in structural traps subject to hydrodynamic conditions. Hubbert's hydrodynamic theory has seen widespread application in the exploration and development of oil and gas fields (Welte and Yukler, 1981; Dahlberg, 1982, Ungerer and others, 1986; Davis, 1987; and England and others, 1987).

Despite the long history of research, few hydrodynamic studies have addressed the basin scale hydrogeology of petroleum migration or implications concerning the history of flow systems. As a result, questions regarding hydrologic mechanisms of transport and timing of petroleum accumulation remain largely unanswered. A notable exception in petroleum migration studies is the work of Tóth (1970, 1978, 1980) who advanced the theory that gravity-induced cross-formation flow is the principal mechanism for the transport and accumulation of hydrocarbons in geologically mature sedimentary basins. Tóth envisaged secondary migration occurring soon after the development of subaerial topographic relief, with migration over tens of kilometers and preferential accumulation of hydrocarbons in areas of quasi-static and ascending groundwater flow.

Conceptual models for the hydraulic theories of petroleum migration stem from parallel studies on the formation of sediment-hosted ore deposits such as those of the Mississippi Valley.[1] Chamberlain (1882) and Daubrée (1887) first proposed circulating groundwaters as the primary agent for concentration of metal sulfides in sediment-hosted ore deposits, as did Van Hise and Bain (1902), Cox (1911), and Siebenthal (1915) in their pioneering studies of the Mississippi Valley. Later theories called upon compaction as the hydrologic mechanism for flow (Noble, 1963; Jackson and Beales, 1967; Dozy, 1970; Sharp, 1978), but

[1] See the paper by Sverjensky (1986) for a review of the geological and geochemical setting.

recently Cathles and Smith (1983) and Bethke (1985) have demonstrated mass balance problems associated with compaction-driven flow. Thermally-driven convection may overcome the mass balance problem of oil and ore deposit genesis (Wood and Hewett, 1984; Rabinowicz, and others, 1985; Blanchard and Sharp, 1985; Jowett, 1986), if thick aquifers act as both source bed and reservoir.

Garven and Freeze (1982, 1984a,b) proposed an alternative hydrologic model for fluid transport in compacted foreland basins. They argued for topography-or gravity-driven groundwater flow at the basin-wide scale as a mechanism for the formation of major ore deposits in discharge zones at edges of foreland basins and along intracratonic basin arches. Hydrogeologic models of gravity-driven flow were used in Garven and Freeze (1984b) to demonstrate a wide range of hydrologic, geologic, and geochemical conditions favorable for stratabound ore genesis. Geologic evidence for this hydrologic model comes from observations on ore mineralization and diagenesis in the midcontinent ore districts of the United States and in the Pine Point ore district of western Canada (Garven, 1985, 1986a; Gregg, 1985; Bethke, 1986; Leach and Rowan, 1986; Hearn, Sutter, and Belkin, 1987; Kaiser and others, 1987).

It seems reasonable to concede that both oil and ore deposits could form solely as the result of long-distance, regional groundwater flow in an uplifted foreland wedge. One goal of this paper is to quantify, in a hydrologic sense, the genetic link between the formation of oil and ore deposits in sedimentary basins (Hitchon, 1977; Eugster, 1985; Oliver, 1986). The major goal, however, is to quantify the massive long-distance migration of oil that was induced by uplift of the foreland in the Western Canada basin (Demaison, 1977, Garven 1986b).

GEOLOGIC SETTING OF THE OIL SANDS DEPOSITS

Enormous volumes of viscous, low-gravity oil exist in a broad belt of deposits situated near the eastern edge of the Western Canada sedimentary basin (fig. 1), a foreland wedge and platform with rocks ranging in age from Cambrian to Quaternary. Bounded on the east by a Precambrian shield, the basin stratigraphy is characterized by a blanket of Cretaceous shale and sandstone unconformably overlying eroded Jurassic, Triassic, and Paleozoic carbonates, shale, and evaporites which dip gently toward the Alberta Foothills (fig. 2). The western boundary of the basin is marked by the edge of the fold and thrust belt of the Rocky Mountains. Much of the present basin structure owes its origin to later phases of the Laramide orogeny which culminated during Eocene time (Porter, Price, and McCrossan, 1982; Beaumont and others, 1985).

Accumulation of heavy oil is concentrated in reservoirs associated with the pre-Cretaceous unconformity (Vigrass, 1968). An estimated total of 2×10^{11} m^3 (1350 billion barrels) of oil exist in sands of the Lower Cretaceous Mannville Group comprising the Athabasca-Wabas-

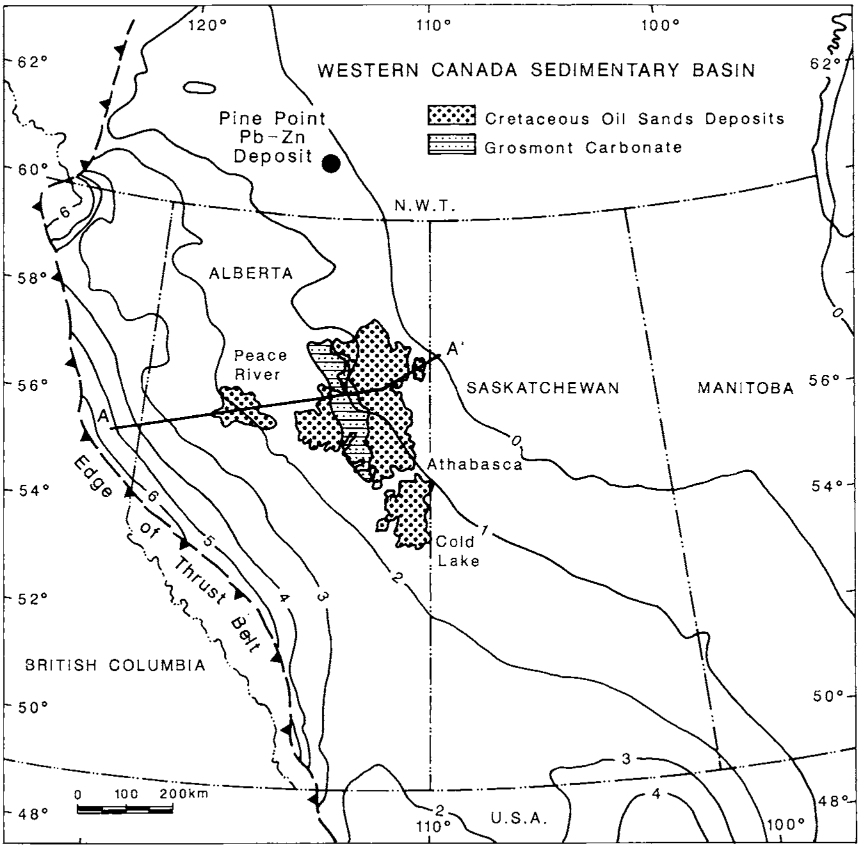

Fig. 1. Isopach map of the Western Canada sedimentary basin and location of the giant oil sands deposits. Line A–A′ denotes the geologic cross section location of figure 2. Contour labels represent kilometer thickness of the sedimentary wedge (after Wright, 1984).

ca, Peace River, and Cold Lake deposits (Mossop, 1980). The Athabasca deposit (fig. 3) forms the largest oil field (1.4×10^{11} m^3). Information concerning stratigraphy, lithology, and hydrogeology are summarized in figure 4 for the Athabasca deposit. Semi-consolidated sands of the McMurray Formation serve as reservoir rock for the oil in the Athabasca deposit with an average pay zone of about 30 m (Mossop, 1980). Geologic considerations indicate that the oil accumulated in early-formed stratigraphic and structural traps at the edge of the basin as a result of long-distance fluid migration (Vigrass, 1968). Little controversy exists with respect to the cause of trapping, but the mechanism responsible for this massive migration of oil is debated. Subsequent water washing and biodegradation has further altered and rendered the

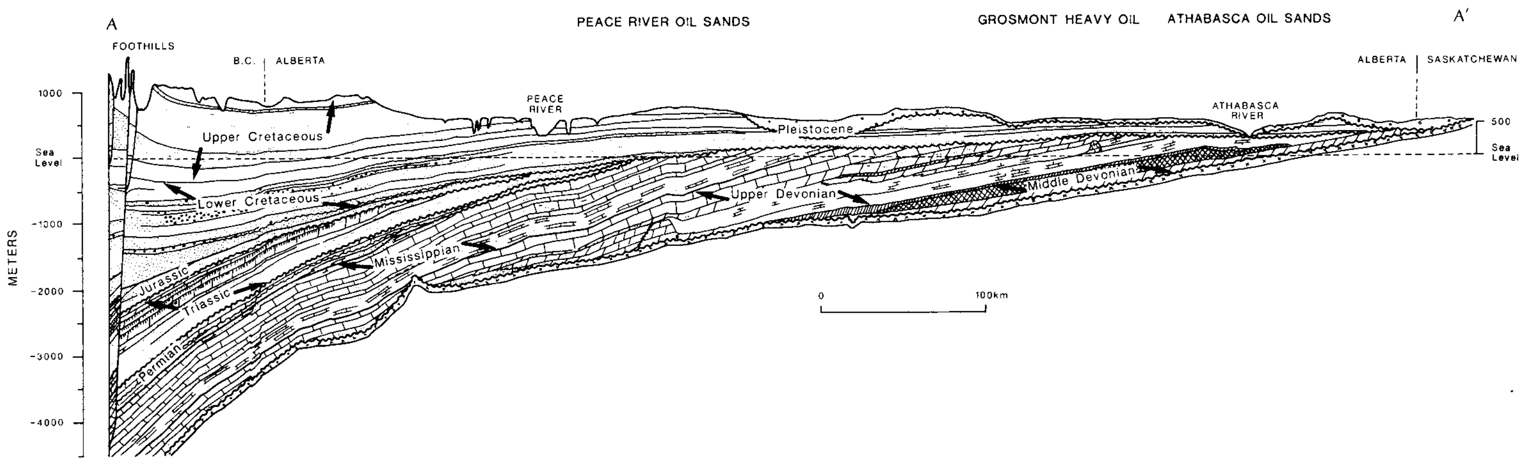

Fig. 2. Geologic cross section of the Western Canada sedimentary basin showing the major stratigraphic units and present-day topographic profile (after Wright, 1984).

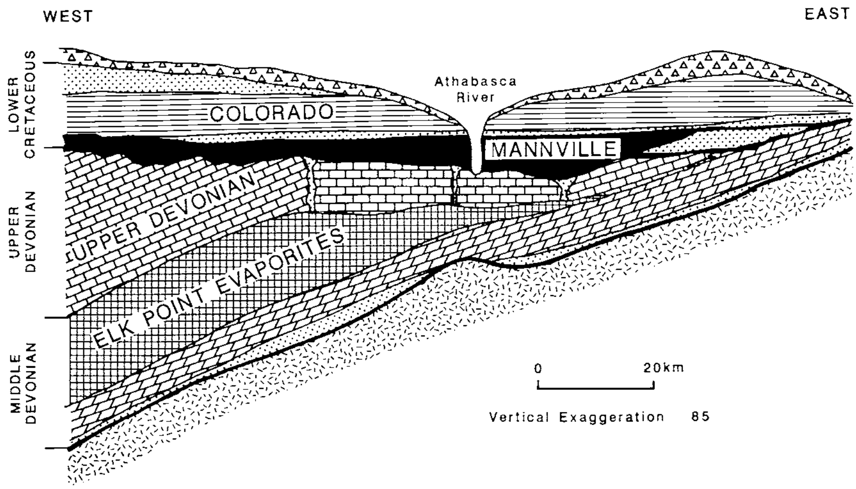

Fig. 3. Expanded view of the geologic habitat of the Athabasca oil deposit. Heavy oil accumulated in the Lower Cretaceous Mannville sands as a result of long-distance migration out of the foreland basin with flow focused in the Upper Devonian carbonate aquifer (geology after Carrigy, 1974).

hydrocarbons to their present immobile state of high specific gravity and viscosity (Rubenstein and others, 1977). In addition to the Mannville Group oil sands, another 2×10^{11} m^3 of bitumen is present in the Paleozoic carbonate trend below the pre-Cretaceous unconformity, the most studied unit being the Upper Devonian Grosmont reef complex (Hoffmann and Strauz, 1986). The combined total volume of heavy oil in Alberta is staggering in comparison to oil fields in other parts of the world. For example, Hunt (1979) reports that Prudhoe Bay contains reserves of 2.4×10^9 m^3 (15 billion barrels), and the Persian Gulf contains an estimated 0.7×10^{11} m^3 (450 billion barrels).

ON THE ORIGIN OF THE OIL SANDS

A critical question to ponder in any genetic model for a giant oil field is the origin of the driving mechanism for fluid migration and timing of accumulation. Numerous theories have been proposed to explain the origin of the Alberta oil sands deposits. Some of the theories are based on geological reasoning alone, whereas others include geochemical correlation of the heavy oils with hydrocarbons from other parts of the sedimentary basin (table 1). According to Hoffmann and Strausz (1986) the oil-sands bitumen is chemically similar to conventional crude oils from deeper parts of the basin, except for changes caused by biodegradation and solutioning. They share the view of many others that the deposits represent the near-surface alteration of a once conventional (light-gravity) supergiant oil field. The source of hydrocar-

NORTHEASTERN ALBERTA – GENERAL STRATIGRAPHY & HYDROGEOLOGY

ERA	PERIOD		STAGE	AGE	THICKNESS	LITHOLOGY	FORMATION	Group	*HYDROSTRATIGRAPHY*
	QUATERNARY		Pleistocene		0 – 60				
MESOZOIC	CRETACEOUS	UPPER	Santonian	82 Ma	365 – 545		LA BICHE	COLORADO	*Regional Aquitard*
MESOZOIC	CRETACEOUS	UPPER	Coniacian						
MESOZOIC	CRETACEOUS	UPPER	Turonian						
MESOZOIC	CRETACEOUS	UPPER	Cenomanian	100 Ma					
MESOZOIC	CRETACEOUS	LOWER	Albian		15		PELICAN	COLORADO	*Regional Aquitard*
MESOZOIC	CRETACEOUS	LOWER	Albian		30		JOLI FOU	COLORADO	*Regional Aquitard*
MESOZOIC	CRETACEOUS	LOWER	Albian		105		GRAND RAPIDS	MANNVILLE	*Regional Aquitard*
MESOZOIC	CRETACEOUS	LOWER	Albian		105 – 150		CLEARWATER	MANNVILLE	*Regional Aquitard*
MESOZOIC	CRETACEOUS	LOWER	Albian	116	45 – 90		McMURRAY (tar sands)	MANNVILLE	*Aquifer & Oil Reservoir*
PALEOZOIC	DEVONIAN	UPPER	Frasnian	350 Ma	180		GROSMONT		*Major Aquifer & Oil Reservoir*
PALEOZOIC	DEVONIAN	UPPER	Frasnian		150 – 395		IRETON		*Regional Aquitard & Potential Source Rock?*
PALEOZOIC	DEVONIAN	UPPER	Frasnian		180 – 215		WATERWAYS		*Regional Aquitard & Potential Source Rock?*
PALEOZOIC	DEVONIAN	UPPER	Frasnian		0 – 23 / 1 – 4		SLAVE POINT AND FT. VERMILION		*Aquifer*
PALEOZOIC	DEVONIAN	MIDDLE	Givetian	360 Ma	0 – 215		MUSKEG	ELK POINT	*Aquitard*
PALEOZOIC	DEVONIAN	MIDDLE	Givetian		60		KEG RIVER	ELK POINT	*Aquifer*
PALEOZOIC	DEVONIAN	MIDDLE	Givetian		75		CHINCHAGA	ELK POINT	*Aquitard*
PALEOZOIC	DEVONIAN	MIDDLE	Givetian				ERNESTINE LAKE	ELK POINT	*Aquitard*
PRECAMBRIAN			Proterozoic	1.7-2.3 billion years	0 – 8		ATHABASCA		*Aquitard*
PRECAMBRIAN			Archean						*Aquitard*
					Meters				

bons is an unresolved problem. For many years geologists accepted the Lower Cretaceous shale as the sole source unit based on chemical correlations, but mass balance calculations have shown that the Mannville Group (fig. 4) could at most account for about 30 percent of the oil sands deposits, excluding the Grosmont bitumen (Moshier and Waples, 1985). It is now clear that this immense amount of hydrocarbons must have originated from numerous distant and diverse parts of the basin in a hydrodynamic system capable of transporting oil not only from mature parts of the Mannville, but also from deeper organic-rich strata such as the Jurassic Nordegg shale, the Mississippian Exshaw and Banff shale, and the Upper Devonian Duvernay shale (table 1). The necessity of long-distance migration appears to be an accepted condition for the origin of the Alberta oil sands, although the nature, timing, and driving force of migration are unknown.

Two types of fluid dynamics models have emerged over the years to explain the accumulation of the heavy oil deposits. The first model considers immiscible phase transport of oil during secondary migration with buoyancy acting as the main driving force. Sproule (1938) and Link (1951) proposed upward oil leakage through fractures and karst channels associated with Devonian reef reservoirs with pooling at the land surface as the Mannville sands were deposited. Demaison (1977) hypothesized separate-phase migration out of the foreland basin in the late Cretaceous with compaction acting as the driving force for expelling hydrocarbons from the Lower Cretaceous section. He also noted the important role of the Cretaceous shale sequence in confining vertical fluid migration in the Alberta basin. Demaison was also one of the first to suggest that basin uplift with thrusting and foreshortening could have initiated a powerful cross-basin groundwater flow system that would enhance oil migration. Du Rouchet (1985) preferred a somewhat different scenario of oil migration with separate-phase flow focused along the sub-Cretaceous unconformity and weathered parts of the Paleozoic bedrock. He proposed bulk migration from Triassic source rocks but offered no explanation for the driving mechanism or timing of oil migration.

The second fluid dynamics model considers miscible transport of oil in molecular and miscellar solution with sediment compaction and topography acting as the driving force for regional groundwater flow. Vigrass (1968) called upon compaction-driven flow with precipitation in the updip sandstone caused by salinity changes. Jones (1980) estimated that compaction would be inadequate in light of the high solubility required (~8,000 ppm). Using the present-day hydrodynamic system (fig. 5) as a conceptual model, Jones reasoned that only 3 ppm oil in solution was needed to account for the giant bitumen deposit, assuming

Fig. 4. Lithology and hydrostratigraphy in northeastern Alberta. Limestone and dolomite in the Upper Devonian constitute the major aquifer in this part of the basin (geology after Jackson, 1975).

TABLE 1

Theories on the origin of the oil sands deposits

Authors	Source Rocks	Nature of Migration	Scale of migration
1. Ball (1935)	Cretaceous shale	Separate phase	Local
2. Sproule (1938)	Paleozoic reservoirs	Separate phase, vertical leakage in fractures	Local to regional
3. Hume (1947)	Cretaceous sands	Derived *in situ*	Local origin
4. Link (1951)	Middle and Upper Devonian reefs	Separate phase, vertical leakage	Local to regional
5. Corbett (1955)	Cretaceous sands	Derived *in situ*	Local origin
6. Gussow (1956)	Paleozoic, deep basin	Separate phase, alteration *en route*	Long distance
7. Hodgson and Hitchon (1965)	Quaternary soils	Derived locally, conversion to heavy oil	Local
8. Vigrass (1968)	Lower Cretaceous	Compaction waters, miscellar solution	Long distance
9. Demaison (1977)	Lower Cretaceous	Separate phase, compaction	Long distance
10. Deroo et al. (1977)	Lower Cretaceous and Paleozoic	Unspecified, but correlation with Mannville	Long distance
11. Hunt (1977)	Mesozoic shales	Compaction waters, molecular solution	Long distance
12. Jones (1980)	Lower Cretaceous, Jurassic shales	Regional groundwater flow, molecular solution	Long distance
13. Leenheer (1983)	Lower Mississippian	Unspecified, but correlation with Exshaw	Long distance
14. Hitchon and Filby (1984)	Upper Devonian shale	Unspecified, but trace element correlation	Long distance
15. Hitchon (1984)	Upper Devonian, Cretaceous shales	Regional groundwater flow, gravity-drive	Long distance
16. Moshier and Waples (1985)	Paleozoic and Mesozoic	Unspecified, but showed Mannville incapable alone	Long distance
17. du Rouchet (1985)	Triassic and Devonian shale	Separate phase flow along sub-Cretaceous unconformity	Long distance
18. Hoffmann and Strausz (1986)	Paleozoic and Mesozoic	Flow in the Paleozoic carbonates, biodegradation	Long distance
19. Garven (this paper)	Paleozoic and Mesozoic	Regional groundwater flow, gravity drive, both miscible and immiscible transport	Long distance

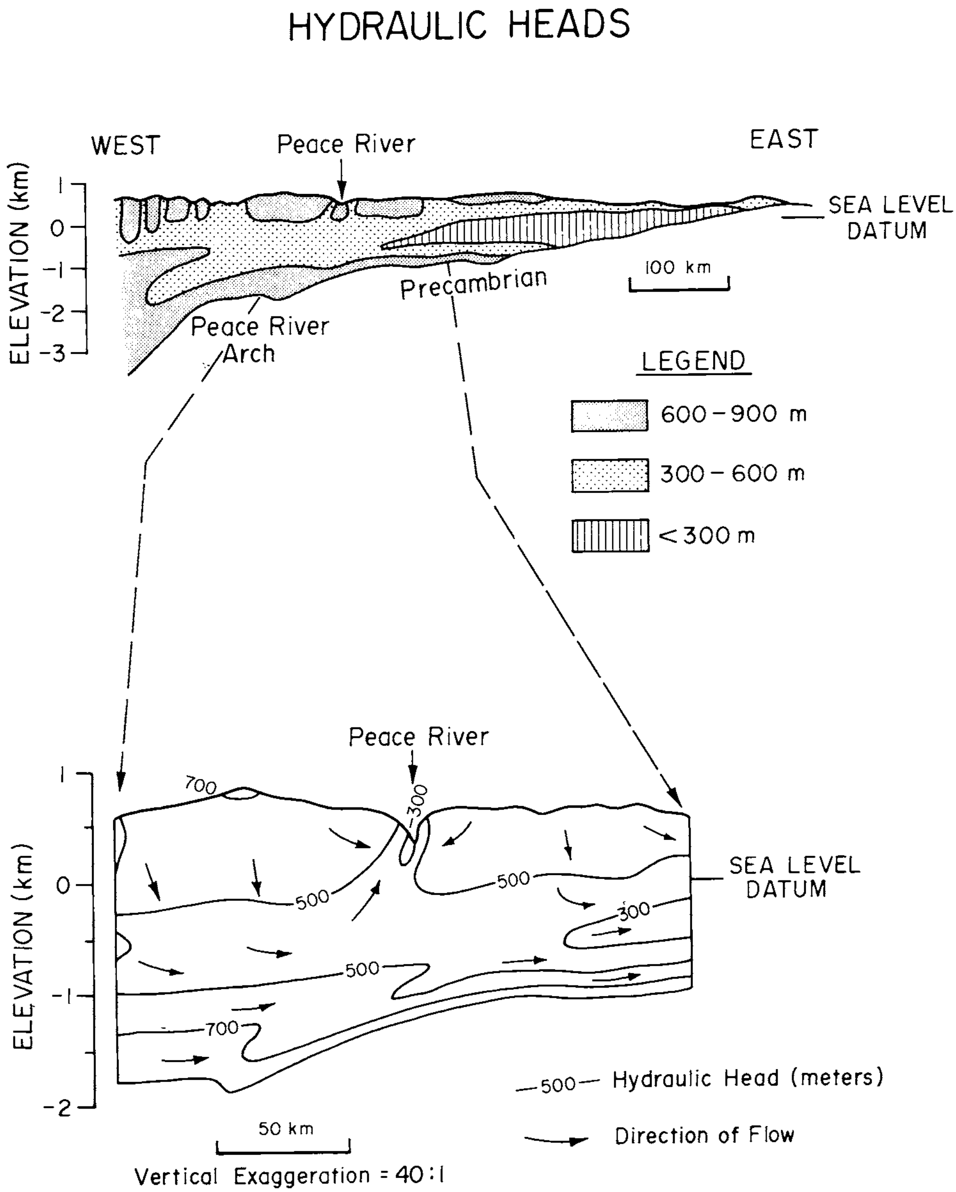

Fig. 5. Present-day groundwater flow patterns in north-central Alberta, near section line A–A′ of figure 1. The hydrodynamic pattern is strongly affected by topography, permeability, and fluid density. This flow system represents a decaying relict of the regional flow created by late Tertiary uplift of the foreland basin (from Garven, 1985—original data after Hitchon, 1969a, 1974).

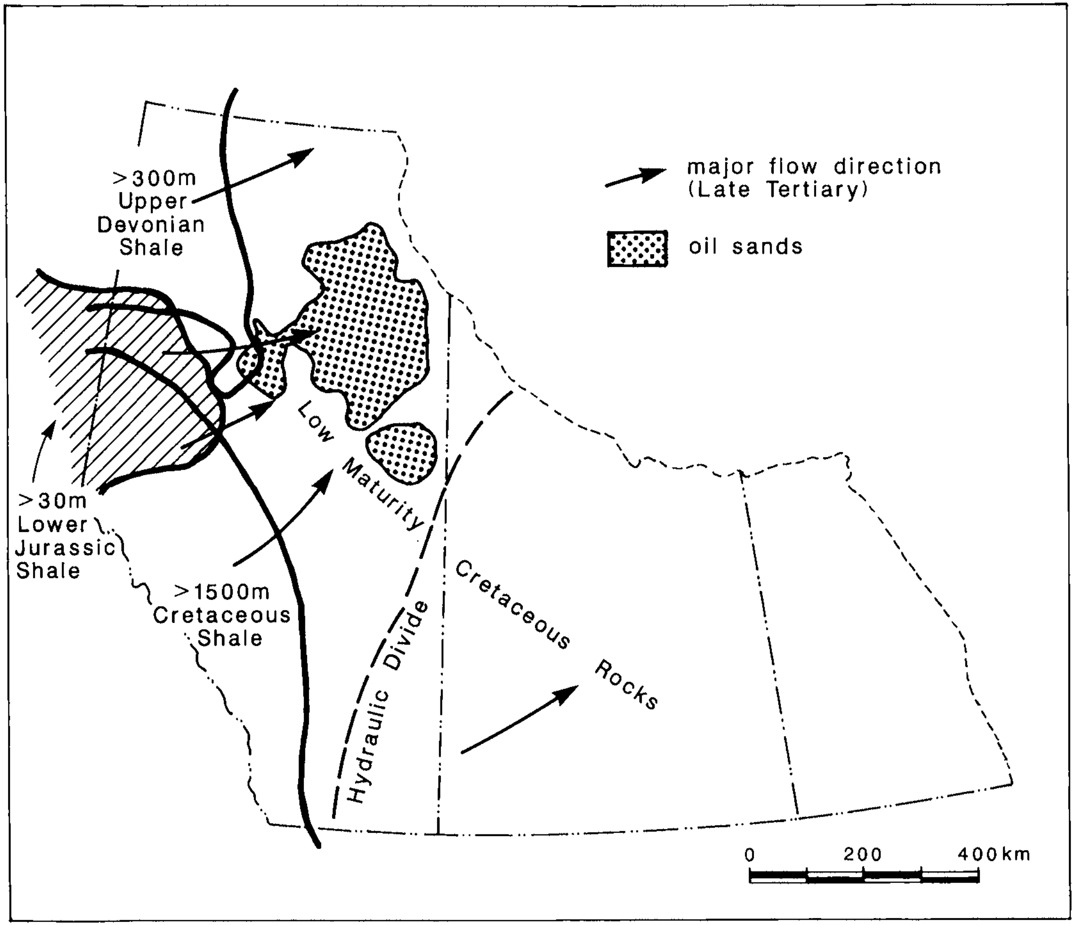

Fig. 6. Hitchon's conceptual model of regional paleoflow and hydrocarbon accumulation in Alberta. The model invokes long-distance migration of oil from widespread source rocks in Devonian and Cretaceous shale (after Hitchon, 1984). The present study proposes additional source rocks in Jurassic strata (shaded on map) which may have controlled the geographical distribution of the oil sand

the flow system operated for 50 million years. Hitchon (1984), Beaumont and others (1985), and Majorowicz and others (1985) have also acknowledged the importance of topography-driven flow in controlling not only oil migration (fig. 6) but also patterns of heating and oil generation.

QUANTITATIVE EVALUATION OF REGIONAL OIL TRANSPORT

Hydrogeologic experiments of hydrothermal fluid flow can be constructed to quantify the role of gravity-driven groundwater flow in the migration and accumulation of hydrocarbons in the Western Canada sedimentary basin. The experimental procedure involves construction of a mathematical model from a conceptual model of the geologic system.

I. *Conceptual Model*

The structural and geologic style of the Western Canada basin can serve as a generic model of a mature basin uplifed by geodynamic forces and beginning a phase of subaerial erosion (fig. 7). Meteoric infiltration sustains the sedimentary pile such that recharge balances groundwater discharge across the basin, and the water table assumes a subdued configuration replicating the topography. Groundwater recharge is concentrated in the elevated parts of the basin where fluids descend to great depth acquiring salinity and heat along the flow path. Major aquifers focus regional flow laterally to discharge areas near the edge of the basin where the brines cool on ascending and mix with shallow-circulating groundwater.

Hydrocarbons enter the flow system in two ways: (1) as a soluble component leached from source regions within the thermally mature portions of the section and precipitated out in regional discharge areas for physiochemical reasons, and (2) as an insoluble component transported in separate-phase as petroleum droplets or continuous slugs. In case (2), buoyancy would force the transport of petroleum to hug the tops of regional aquifers, and trapping would occur wherever or whenever the forces of buoyancy and capillarity exceeded the impelling force of the groundwater flow (Hubbert, 1953; Tóth, 1980). The flow paths inferred here (fig. 7) assumes a negligible hydraulic gradient orthogonal to the topographic slope, an assumption aided by the large ratio of length to width in foreland basins (fig. 1). Fluid circulation is bounded along the width of the basin by the fold and thrust belt on one side, which would create a near vertical barrier, and by the erosional edge of the sediments on the other side. The depth of regional flow is mapped at the crystalline basement contact, although there is no hydrologic reason why basinal brines could not circulate in the weathered and jointed zone near the unconformity.

The model portrayed above is similar in concept to the hydrologic theories noted earlier, except that greater emphasis has been placed on the role of groundwater flow, the nature of petroleum transport, and the scale of migration. The model is unconventional in two areas with

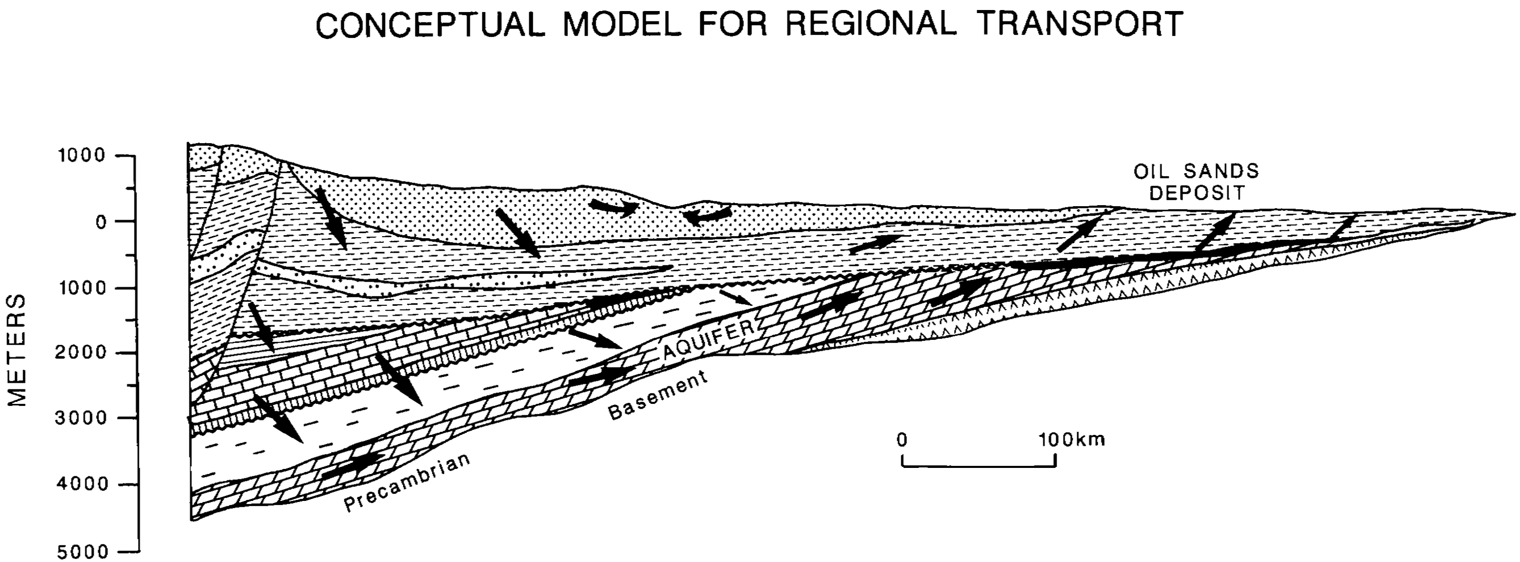

Fig. 7. Conceptual model of gravity-driven groundwater flow in a compacted and uplifted foreland basin. Descending groundwater in the elevated portion of the basin leaches soluble oil near deeply buried source rock with focused transport into regional aquifers. Separate-phase oil enters aquifers but from below and is impelled by the groundwater system. Accumulation of giant oil deposits occurs in the discharge end of the regional flow system because of oil precipitation on cooling and trapping as a separate phase. The shale aquitard is impermeable to separate-phase oil but not to groundwater.

respect to the accepted theory on petroleum formation and migration (Tissot and Welte, 1978; Magara, 1986): (1) it does not call upon compaction as the mechanism driving flow; (2) it supports the possibility for soluble petroleum transport in long-distance migration (Price, 1976). The mass balance problems of compaction have already been described by Jones (1980) and Garven (1985) for the case of the Western Canada basin. Great debates exist on the viability of transporting hydrocarbons in solution because of the limited solubility under reservoir conditions (fig. 8), especially for the heavier compounds common in crude oils (McAuliffe, 1980). However, given the range of solubilities possible, it seems plausible that miscible transport has played an important role in the formation of the oil sands.

II. *Mathematical Formulation*

Multiphase fluid flow, heat transfer, and chemical mass transport are satisfactorily treated with continuum theory for porous media (Bear, 1972), although limitations always exist in the representation of fractured rock and the scale effect of heterogeneities in sedimentary basins (Garven, 1986a). Table 2 summarizes the mathematical model constructed for this study. The dependent variables in eqs (1) through (10) include: reference state hydraulic head h_w and petroleum head h_o, elevation above reference datum Z, Darcy velocity of groundwater q_w and oil q_o, average linear velocity of groundwater v_w and oil v_o, fluid

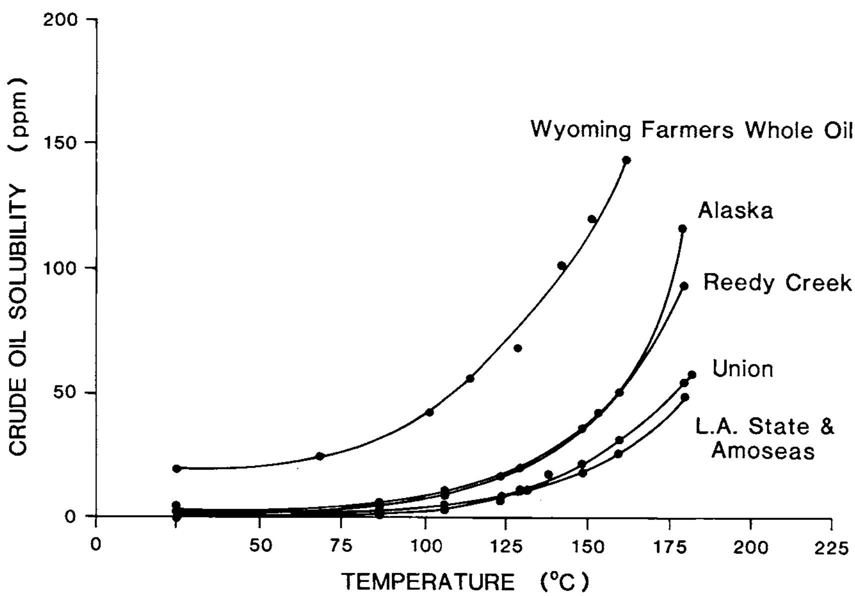

Fig. 8. Solubility of crude oils in dilute water as a function of temperature (after Price, 1976).

TABLE 2
Transport equations

Darcy's law		
	$\mathbf{q_w} = -\mathbf{K_w}\mu_{rw}(\nabla h_w + \rho_{rw}\nabla Z) = \mathbf{v_w}\phi$	(1)
	$\mathbf{q_o} = -\mathbf{K_o}\mu_{ro}(\nabla h_o + \rho_{ro}\nabla Z) = \mathbf{v_o}\phi$	(2)
Conservation of fluid mass		
	$-\nabla \cdot (\rho_w \mathbf{q_w}) = \frac{\partial(\phi\rho_w S_w)}{\partial t} + \Gamma_w$	(3)
	$-\nabla \cdot (\rho_o \mathbf{q_o}) = \frac{\partial(\phi\rho_o S_o)}{\partial t} + \Gamma_o$	(4)
Conservation of groundwater vorticity		
	$\nabla \cdot \left[\frac{\mathbf{K}}{\lvert\mathbf{K}\rvert}\mu_w \nabla\Psi\right] = -g\frac{\partial\rho_w}{\partial x}$	(5)
Conservation of hydrothermal energy		
	$\nabla \cdot [\mathbf{E}\nabla T] - \rho_w c_w \mathbf{q_w} \cdot \nabla T = [\rho_w c_w \phi + \rho_s c_s(1 - \phi)]\frac{\partial T}{\partial t}$	(6)
Conservation of soluble oil mass		
	$\nabla \cdot [\mathbf{D}\nabla C_o] - \mathbf{v_w} \cdot \nabla C_o = \frac{\partial C_o}{\partial t} + \sum_r \nu_{or} R_r$	(7)
Conservation of insoluble oil mass		
	$-\mathbf{v_o} \cdot \nabla m_o = \frac{\partial m_o}{\partial t}$	(8)
Equations of state		
	$\rho_w = \rho_w(p,T,\omega)$ and $\mu_w = \mu_w(p,T,\omega)$	(9)
	$\rho_o = \rho_o(p,T,\omega)$ and $\mu_o = \mu_o(p,T,\omega)$	(10)

generation rate for water Γ_w and oil Γ_o, saturation content of water S_w and oil S_o, groundwater stream function Ψ, groundwater temperature T, concentration of aqueous oil C_o, rate of reaction of aqueous oil R_r, mass of oil in separate phase m_o, fluid pressure p, and groundwater salinity ω. Hydrogeologic properties that must be specified are the hydraulic conductivities of the rock for water K_w and oil K_o, porosity ϕ, thermal conductivity-dispersion coefficient E, specific heat capacity c, and the solute dispersion coefficient D. Fluid density ρ and viscosity μ are dependent functions of pressure, temperature, and salinity. Other variables and parameters are defined in the symbol notation list.

Regional fluid flow in the conceptual model of the mature foreland basin is considered as a steady-state flow problem, and therefore the transient terms in eqs (3) and (4) can be neglected. The steady state assumption implies that the water-table configuration remains in a similar form over long periods of geologic time (Freeze and Witherspoon, 1967). Moreover, transient pore pressures caused by compaction, uplift, and erosion are assumed to have dissipated (Neuzil and Pollock, 1983; Neuzil, 1986). Local transients induced by changes in the water saturation S_w would occur in regions of separate oil-phase accumulation, but we will assume these transients have a negligible effect on groundwater flow at the basin scale. The amounts of fluid generated from the release of water by clay mineral reactions Γ_w and from the conversion of kerogen to oil Γ_o are taken here to be negligible in comparison to the immense volume of groundwater driven across the basin by topography. The treatment of multiphase flow incorporates nonlinear effects into (3) and (4) because of the dependency of the permeability and hydraulic conductivity on the relative saturation contents of the fluids. The nonlinear condition can be relaxed, if it is assumed that the separate-phase oil exists as small discontinuous globules and slugs in an otherwise water-saturated, very permeable media (Hubbert, 1953). Under these conditions, capillary forces are very small and petroleum migration is dominated by the impelling force of the groundwater, modified by the effects of buoyancy. Eq (2) in table 2 can be simplified by following the approach of Hubbert (1953, eq 41) and defines:

$$\mathbf{E}_o = \mathbf{g} + \frac{\rho_w}{\rho_o}(\mathbf{E}_w - \mathbf{g}) \tag{11}$$

where, $\mathbf{E}_o$ is the driving force of the oil, $\mathbf{E}_w$ the driving force of the groundwater, and $\mathbf{g}$ is the gravitational body force (0, 0, -g), all per unit mass of fluid. The respective fluid flow rates can be expressed as (Hubbert, 1953, eq 17):

$$\mathbf{q}_w = \sigma_w \mathbf{E}_w \tag{12}$$

and

$$\mathbf{q}_o = \sigma_o \mathbf{E}_o \tag{13}$$

where σ is a proportionality constant (K/g). It follows from (11) that:

$$\mathbf{q}_o = \sigma_o \left[\mathbf{g} + \frac{\rho_w}{\rho_o}(\mathbf{E}_w - \mathbf{g})\right] \tag{14}$$

and therefore,

$$\mathbf{q}_o = \frac{\rho_w \sigma_o}{\rho_o \sigma_w}\mathbf{q}_w - \sigma_o \mathbf{g}\left(\frac{\rho_w}{\rho_o} - 1\right) \tag{15}$$

Assuming the effective intrinsic permeabilities of the aquifer are the same for water and oil, eq (15) can be reduced to a form written as a function of the water velocity and buoyancy effect:

$$\mathbf{q}_o = \frac{\mu_w}{\mu_o}\mathbf{q}_w + \mathbf{K}\left(\frac{\rho_w - \rho_o}{\rho_o}\right)\nabla Z \tag{16}$$

Keep in mind that eqs (11) through (16) are strictly valid only for oil migration in a permeable aquifer, and they would not hold for less permeable strata where forces of capillarity dominate (Anderson, 1987).

A fluid potential per unit weight, or petroleum head h_o, can be calculated from the groundwater potential field by modifying Hubbert's original equation for the petroleum force potential per unit mass (Hubbert, 1953, eq 40). The result becomes:

$$h_o = \frac{\rho_w}{\rho_o} \cdot h_w - \left(\frac{\rho_w - \rho_o}{\rho_o}\right)Z \qquad (17)$$

where the symbols are defined as before. The petroleum head and the oil velocity vector are easily computed with (17) and (16), once eqs (1) and (3) are solved. Pathlines for groundwater flow are conveniently represented by the stream function Ψ (discharge rate per unit width) in eq (5) which is derived from the circulation of inhomogeneous fluid flow (Bear, 1972, p. 241).

Eq (6) accounts for thermal conduction in the rock and water and for convective and dispersive heat transfer caused by groundwater flow. Heat transport associated with advection of oil or with chemical reactions is assumed to be insignificant. Equation of state (10) allows for the modeling of both free and forced convection with (3) or (5) because of the coupling with (6) through water density. For the case of long-term steady flow in the sedimentary basin, the heat transport equation can be simplified to a steady form by eliminating the transient term (Garven and Freeze, 1984a).

Conservation of soluble oil mass in the flowing groundwater is described with a form of the advection-dispersion equation (7) modified for dissolution-precipitation reactions and biodegradation. The solute transport equation accounts for both advection and mechanical dispersion of the dissolved oil in the aquifer. In theory, eq (7) could be used to model the primary migration of oil by diffusion from kerogen-rich source beds. Separate-phase oil migration could be rigorously modeled by the simultaneous solution of eqs (1) to (4), provided the characteristic curves relating permeability and capillary pressure versus fluid saturation contents are known for all rocks in the basin (Peaceman, 1977). As that approach is outside the scope of the paper, eq (16) provides a suitable alternative for the problem at hand. Discrete volumes of oil can still be tracked in the flow system by solving for the rate of oil mass advection with (8) which represent a continuity form of the Buckley-Leverett equations (Bear, 1972).

The final step in formulating the mathematical model is specification of boundary conditions. Table 3 outlines the boundary surface conditions for the conceptual model in mathematical notation, where **n** is the outward pointing unit vector, **r** is the surface tangent unit vector, **q** is the Darcy velocity, **J** is the conductive heat flux, and **F** is the dispersive-diffusive mass flux. The water table is a surface of free mass flow, and it is isothermal and isobaric. Near vertical hydraulic divides

TABLE 3

Mathematical boundary conditions

Surface	Hydraulic	Thermal	Oil Mass
Water table	$h_w = Z$ and $\left(\frac{1}{\lvert\mathbf{K}\rvert}\mathbf{K}\nabla\Psi\right)\cdot\mathbf{n} = -\nabla h_w \cdot \mathbf{r}$	$T = T_0$	$\mathbf{v}\cdot\mathbf{n}\nabla C = 0$
Basin edge	$\mathbf{q}\cdot\mathbf{n} = 0$ and $\Psi = 0$	$\mathbf{J}\cdot\mathbf{n} = 0$	$\mathbf{F}\cdot\mathbf{n} = 0$
Thrust front	$\mathbf{q}\cdot\mathbf{n} = 0$ and $\Psi = 0$	$\mathbf{J}\cdot\mathbf{n} = 0$	$\mathbf{F}\cdot\mathbf{n} = 0$
Basement	$\mathbf{q}\cdot\mathbf{n} = 0$ and $\Psi = 0$	$\mathbf{J}\cdot\mathbf{n} = J_B$	$\mathbf{F}\cdot\mathbf{n} = 0$

would be created at the leading edge of the fold and thrust belt and at the feather edge of the platform; therefore they are modeled as no-flow boundaries for fluids, heat, and mass transport. The basement unconformity also serves as a barrier to fluid flow and solute mass transport, but heat flow from the underlying crystalline crust enters at a nearly constant rate.

III. *Numerical Formulation*

Numerical solutions are required for the mathematical model due to the absence of closed-form analytical solutions for the coupled fluid flow, heat, and mass transport problem. Details concerning the numerical methodology can be found in the appendix. Although simplifications are required in the scale of discretization of the geologic framework, numerical methods provide the most practical means of obtaining solutions to the transport equations for two-dimensional flow in sedimentary basins. The geologic cross section is first discretized, and the appropriate material properties and boundary conditions are specified. A salinity-depth profile is specified and initial conditions for the fluid properties are determined from the conductive temperature field. Water density and viscosity are computed from fitted equations of state (Kestin, Khalifa, and Correia, 1981). The finite element method is used to solve the coupled groundwater flow, stream function, and heat transport equations. With the hydraulic heads computed, petroleum (oil) heads are calculated with eq (17) and the Darcy velocity vectors for the two fluids are then computed with (1) and (16). Hydrocarbon mass transport is simulated with a moving-particle random-walk method, with advection and dispersion for the miscible case, but only advection for the immiscible case. The particle-tracking technique can also model changes in petroleum mass caused by oil generation and biodegradation along the flow path, although no reactions are considered in the present study.

IV. *Numerical Simulations*

A series of paleohydrologic simulations are presented here to investigate the role of regional groundwater flow in the transport and accumulation of hydrocarbons in the giant oil sands deposits of the Western Canada sedimentary basin. Firstly, the hydrodynamic setting is calculated for steady-state representations of the groundwater and oil flow fields, as well as for the thermal regime in the basin (figs. 9–16). Secondly, a mass transport simulation is described for oil migration in aqueous solution in a regional aquifer (fig. 17). Finally, mass transport simulations are presented for oil migration as separate-phase slugs (figs. 19 and 20).

Hydrogeologic model.—The paleogeologic section representing late Eocene time extends west-east from the present-day foothills to the Precambrian shield (fig. 9A). This line of section roughly coincides with A – A′ in figure 1, the direction of the inferred topographic gradient and known direction of fluid flow in the Holocene system (Hitchon, 1969a,b). The modeled basin extends laterally for 724 km, and thickness ranges from over 6100 m at the thrust front to about 500 m at the eastern margin. The configuration of the water table is taken as a linear decline for purposes of simplicity with a slope of 0.2 percent from west to east. This slope probably represents a minimum value based on the present topography (fig. 2) and estimates of erosion that followed the Laramide orogeny (Hacquebard, 1977; Nurkowski, 1984).

Nine hydrostratigraphic units are used to characterize the regional hydrogeology of the foreland basin (fig. 9A). This subdivision is largely based on the stratigraphy and lithology (McCrossan and Glaister, 1964; Porter, Price, and McCrossan, 1982) and hydrogeology (Hitchon, 1969a,b; Tóth, 1978; Garven, 1985). Assumed paleovalues of the controlling parameters are listed in table 4 for each hydrostratigraphic unit. Weathered and dolomitized carbonates of Upper Devonian age (unit 4) constitute a major regional aquifer in the basin model, as does the Middle Devonian Keg River Formation (unit 1). A horizontal hydraulic conductivity $K = 200$ m/yr ($k = 650$ millidarcys, md) is assumed for both aquifer units, a reasonable value for the regional permeability of vuggy and fractured carbonates in the Western Canada basin (Thomas, 1962; Garven, 1985, 1986a). The Lower Cretaceous Mannville sands (unit 9) would also constitute a very permeable aquifer, but as they are the host for the oil deposits, only a moderate hydraulic conductivity of 30 m/yr is assigned. Carbonates and sandstone of the Mississippian-Permian sequence (unit 6) are assigned a similar permeability, because du Rouchet (1985) proposed that these rocks acted as carrier beds for oil accumulation in the Peace River deposit. All the shale-type units are potential source rocks for petroleum and are assigned a vertical hydraulic conductivity on the order of 10^{-1} m/yr (0.03 md) or less for the regional scale. A value of 10^{-5} m/yr is assigned to the bedded evaporites of the Elk Point Group (unit 2). Estimates of porosity, specific storage, hydraulic anisotropy, thermal conductivity, and dispersivity are derived from the data compilations in Tóth (1978), Freeze and Cherry (1979), Garven and Freeze (1984b), and Garven (1985, 1986a). Shales of the Mannville Group (unit 8) are permeable to groundwater and brine flow but are assumed to be impermeable to separate-phase oil migration because of capillarity forces created by the change in lithology at the shale/sand interface (see eq 37, Hubbert, 1953).

Discretization of the hydrostratigraphy is accomplished using 1534 finite elements (fig. 9B). One result of the numerical scheme (see app.) is that functions such as hydraulic head and temperature are continuous from element to element, but flux terms such as the Darcy velocity and the Fourier heat flow become discontinuous on element boundaries. The grid used here is designed to reduce this error by increasing the mesh resolution in areas of steeply changing hydraulic and thermal gradients.

Figure 9C to F displays the computed fluid flow fields using the model parameters in table 4. The groundwater flow field is influenced by both the temperature and salinity field of the basin. One limitation of this numerical model is that salinity of brines are not allowed to be influenced by the flow field. In figure 9D the salinity field is fixed at a constant linear gradient such that the salt concentration reaches a maximum of 40 percent equivalent weight NaCl at the deepest point in the basin. Groundwater descends over about half the basin width and turns to ascend at around the 300 km scale mark on the horizontal axis (fig. 9D). Average linear velocities of the groundwater on the order of 10^{-1} m/yr or less occur in the regional recharge area, but focusing on flow in the Upper Devonian aquifer allows for lateral velocities as high as 8 m/yr near the sub-Cretaceous unconformity. This converts to a Darcy flow rate of 1.6 m/yr in the Upper Devonian aquifer. Darcy flow rates of 10^{-1} and 10^{-5} m/yr are predicted for the Middle Devonian Keg River Formation aquifer and Elk Point Group aquitard, respectively. Ascending groundwater crosses the Cretaceous shale over a large area at diffuse rates of 10^{-2} m/yr.

For discrete globules or stringers of oil, the flow field is greatly modified due to the effect of buoyancy (fig. 9E and F). The oil phase is assumed to have a constant density of 850 kg/m^3 and viscosity of 2×10^{-3} Pa·s in this simulation. No corrections have been made for temperature or pressure on oil viscosity or density for this first-order model. The Darcy velocity of oil reaches a maximum of 0.8 m/yr in the Upper Devonian aquifer, where there is about a three-fold increase in the vertical component of flow relative to the groundwater case (fig. 9F). The petroleum flow field (fig. 9F) shows only the potential for oil migration under the influence of buoyancy and hydraulic drive. Neglection of capillarity in the mathematical model (table 2) restricts realistic predictions to flow in the Devonian aquifers only. For example, upward pointing velocity vectors in the vicinity of the Mannville sands imply the potential for upward flow, but capillarity forces would effectively prevent upward migration of oil into overlying shale and therefore provide the trap for oil accumulation (Vigrass, 1968).

Figure 9, G and H, illustrates the predicted groundwater flow pathlines and temperature field. Groundwater flow is stongly focused by the Upper Devonian aquifer, as noted earlier, and this in turn affects

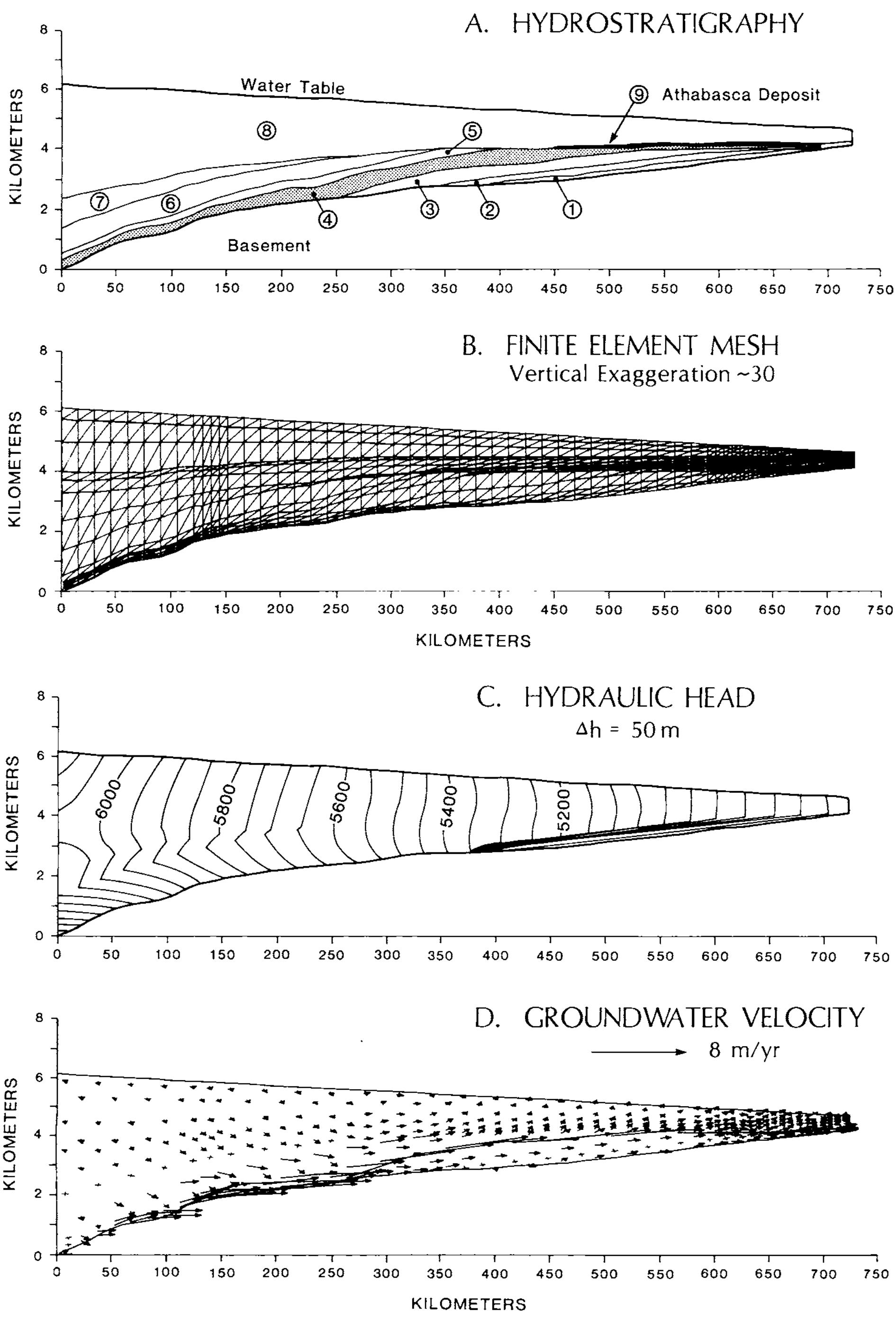

Fig. 9. Hydrogeologic model of Tertiary-time paleoflow in the western Canada sedimentary basin.

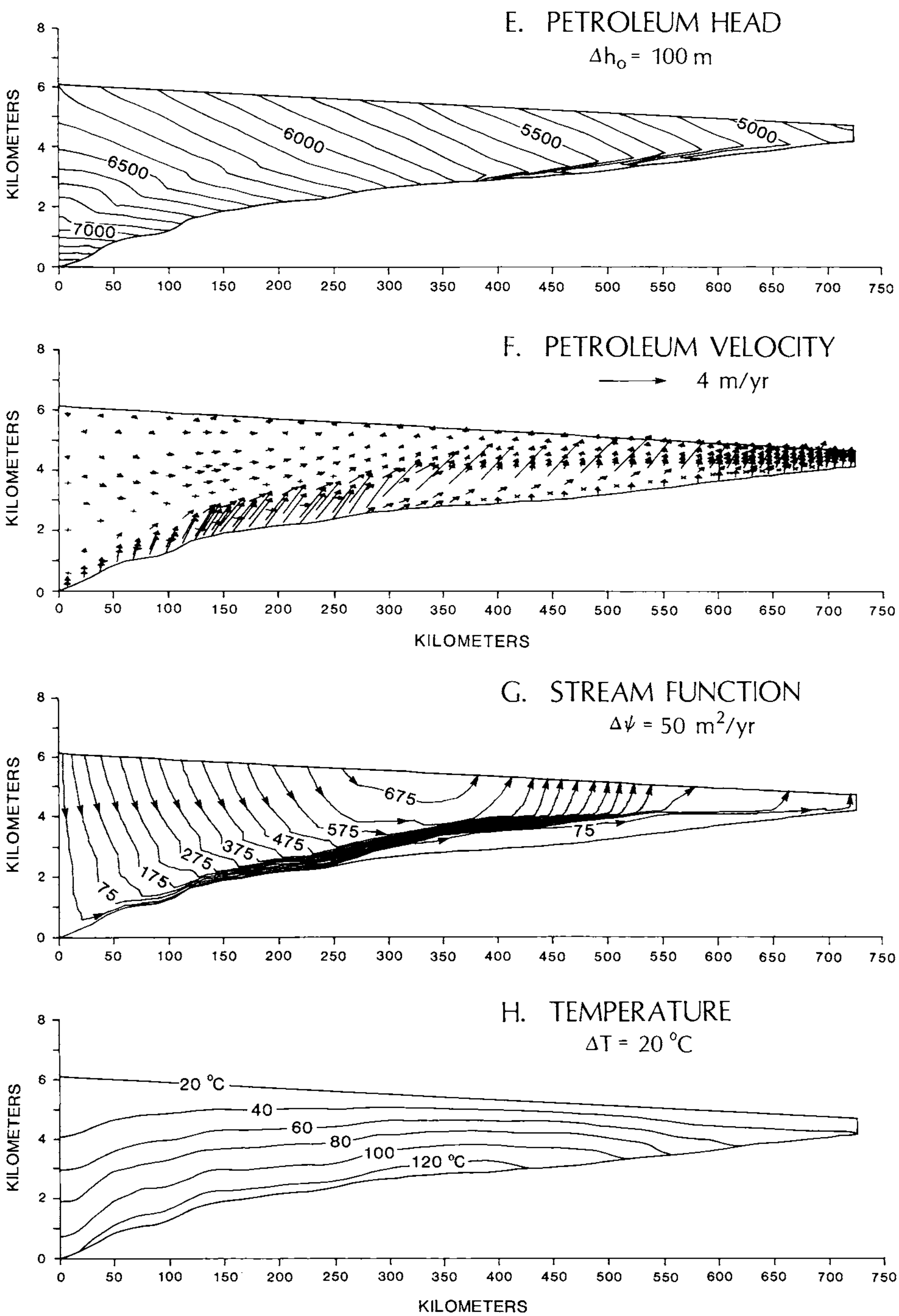

Fig. 9. (continued)

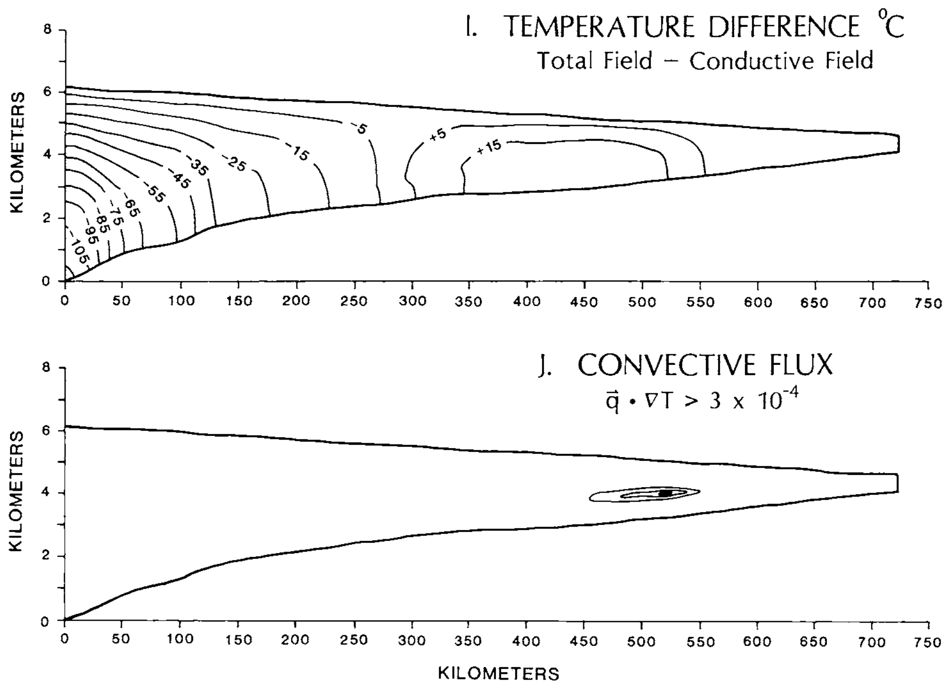

Fig. 9. (continued)

heat transport due to forced convection. Total groundwater flow across the basin is about 710 m^3/yr per meter width in this simulation, with 80 percent of this flow focused through the aquifer along the sub-Cretaceous unconformity and across the Mannville sand unit. Forced convection by the regional flow system elevates temperature relative to the conductive field in the discharge area and depresses temperatures in the recharge area (fig. 9H and I). The effect of convection is noticeably large in the region of greatest discharge at the sub-Cretaceous unconformity (fig. 9J), which could become a zone of intense deposition of oil from solution (Wood and Hewett, 1984).

Parametric study.—A sensitivity study also was undertaken to examine the effects of reasonable variations in the model parameters on fluid flow and heat transport in the Western Canada basin. In figure 10 the hydraulic conductivity of the Upper Devonian carbonate aquifer (unit 4) is varied over three orders of magnitude. The presence of this high permeability unit is clearly visible by the focusing and crowding of fluid flowlines (fig. 10F), but the focused pattern becomes diffuse as the permeability contrast with the surrounding shale and carbonates is decreased for lower ranges in the hydraulic conductivity (fig. 10A). Although the recharge/discharge character of the flow system still

TABLE 4
Model parameter data

Hydrostratigraphic Unit	Porosity (fraction)	Specific Storage Coefficient (m^{-1})	Regional permeability: Horizontal Hydraulic Conductivity (m/yr)	Regional permeability: Vertical Hydraulic Conductivity (m/yr)	Thermal Conductivity (Watts/m °C)	Longitudinal Dispersivity (m)	Transverse Dispersivity (m)
9. Lower Cretaceous Mannville sands	0.30	1×10^{-3}	*3×10^{1}	3×10^{-1}	3.1	1.0	0.1
8. Lower and Upper Cretaceous shale and sandstone	0.15	1×10^{-3}	1×10^{1}	1×10^{-1}	2.1	0.1	0.1
7. Triassic-Jurassic shale and red beds	0.10	1×10^{-4}	1×10^{0}	1×10^{-2}	3.1	0.1	0.1
6. Mississippian-Permian carbonates	0.10	1×10^{-3}	3×10^{1}	3×10^{-1}	3.1	1.0	0.1
5. Lower Mississippian shale and carbonates	0.10	1×10^{-4}	1×10^{1}	1×10^{-1}	2.1	0.1	0.1
4. Upper Devonian carbonates	0.20	1×10^{-3}	2×10^{2}	2×10^{0}	3.1	1.0	0.1
3. Upper Devonian shale, carbonates	0.10	1×10^{-4}	1×10^{1}	1×10^{-1}	2.1	0.1	0.1
2. Middle Devonian evaporites	0.05	1×10^{-5}	1×10^{-3}	1×10^{-5}	4.6	0.1	0.1
1. Middle Devonian carbonates	0.20	1×10^{-3}	2×10^{2}	2×10^{0}	3.1	0.1	0.1

*30 m/yr = 10^{-6}m/s ≈ 10^{-13}m^2 = 100 millidarcys

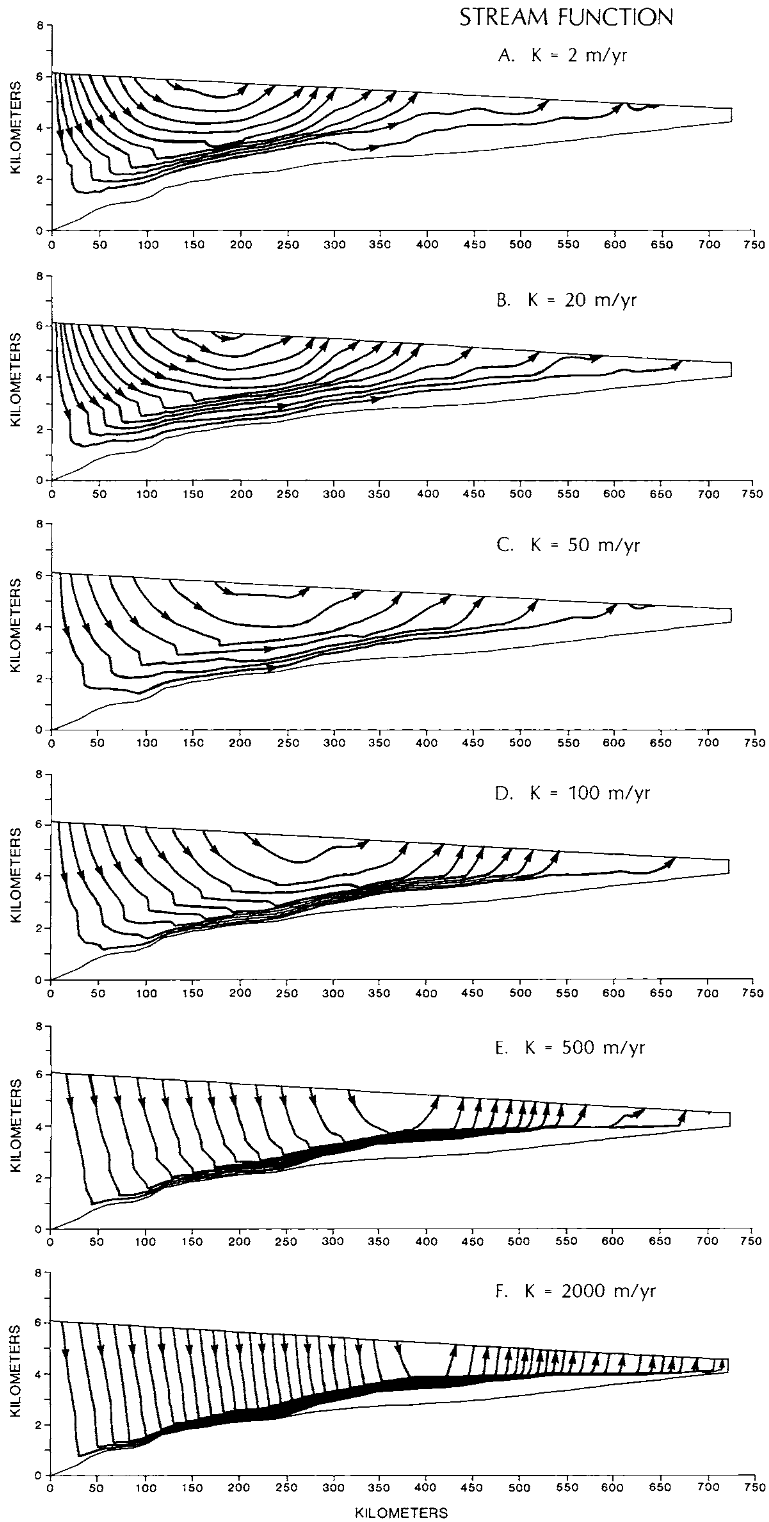

Fig. 10. Effect of aquifer permeability on regional groundwater flow. Parameter K is the horizontal component of the hydraulic conductivity for the Devonian aquifers. Streamline contour interval is 25 m^2/yr in simulations A and B, 50 m^2/yr in C and D, and 100 m^2/yr in E and F.

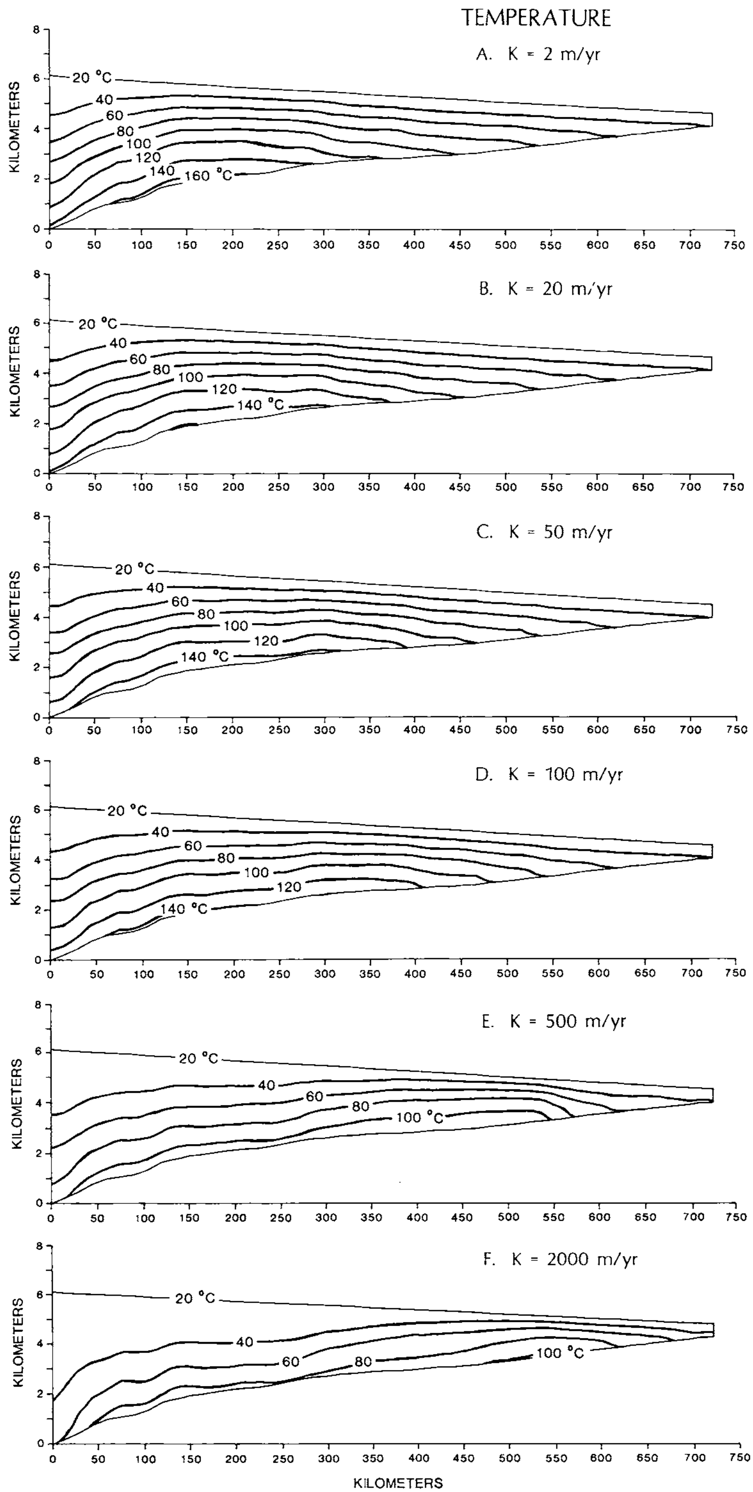

Fig. 11. Effect of aquifer permeability on regional heat flow. Fluid flow patterns are identical to those of figure 10. A heat flux of 70 mW/m^2 is applied along the basement in all simulations.

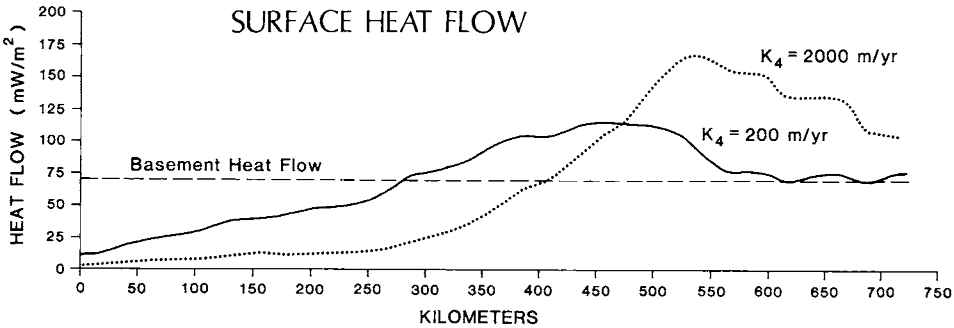

Fig. 12. Heat flow along the top surface of the numerical grid. Parameter K_4 represents the horizontal component of hydraulic conductivity in unit 4 (Upper Devonian aquifer). The plotted curves are computed from the heat flow distribution of figures 9H and 11F. Groundwater flow reduces heat flow in the recharge end of the basin and increases heat flow relative to conduction in the discharge end of the basin.

exists for the lower permeability range (fig. 10A, B, C), massive transport of hydrocarbons would only be effective where sufficient hydraulic contrast exists to focus fluid migration.

The higher rates of groundwater flow associated with the higher range of hydraulic conductivity (fig. 10D, E, F) result in a greater disturbance of heat flow across the sedimentary basin (fig. 11). Quantitative representation of the ratio of advective to conductive heat transport can be expressed as a Peclet number P_e.[2] For figure 9H the $P_e = 0.3$, whereas for figure 11F the $P_e = 1.5$ for a ten-fold increase in aquifer permeability. The disturbance in heat transport caused by regional groundwater flow can be visualized also as anomalies in near-surface heat flow (fig. 12), which largely reflect the subsurface recharge/discharge patterns of groundwater flow (Hitchon, 1984). Heat transport is dominated by conduction in the cases of low-permeability diffuse flow in which no anomalies would appear.

The rate of groundwater flow across the basin is not solely controlled by the hydraulic characteristics of the aquifer focusing flow. In figure 9G the streamline pattern is constrained also by the permeability of stratigraphic units surrounding the Devonian aquifers. Figure 13 displays a series of simulation results in which the hydraulic conductivity of the less permeable strata have been decreased by factors ranging from 2 to 50, relative to the hydraulic parameters of figure 9. Total flow through the basin varies from about 600 m^3/yr per meter width in figure 13A to less than 150 m^3/yr in figure 13E. Lowering the aquitard permeability even further results in unstable flow conditions as thermally-driven free convection begins to occur within the aquifer.

[2] $P_e = [\rho_w c_w Q]/[\lambda_e(L/H)]$ where Q is the total groundwater discharge, λ is thermal conductivity, L is basin length, and H is mean depth (van der Kamp, 1984)

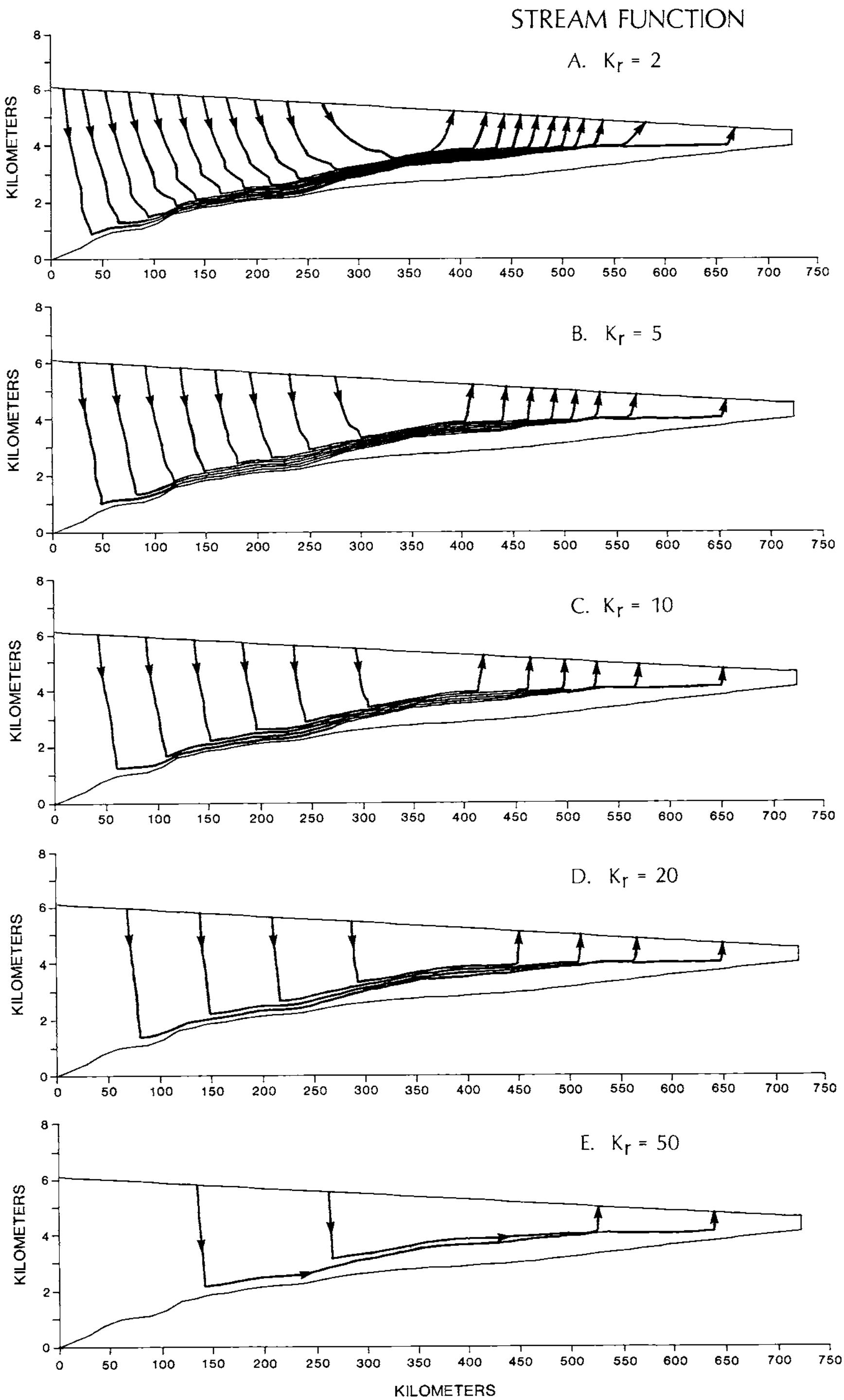

Fig. 13. Effect of aquitard permeability on groundwater flow. Parameter K_r is the ratio of the hydraulic conductivity of the non-aquifer strata in the simulation to the base-case simulation hydraulic conductivity of table 4 and figure 9. The streamline contour interval is 50 m^2/yr in each graph.

The topology of flow patterns in a sedimentary basin is also controlled by the degree of hydraulic anisotrophy in the principal permeabilities. The anisotropy ratio K_x/K_z can range up to several orders of magnitude (Freeze and Cherry, 1979), depending on lithologic variations and the scale of hydrologic analysis (Garven, 1986a). An anisotropy ratio of 100 was used to compute the flowlines of figure 9G. Other numerical simulations have been performed for a wide range of ratios by simultaneously altering the vertical permeability in all stratigraphic units (fig. 14). Higher values of K_x/K_z (larger vertical permeability) result in a slight increase in vertical flow, while lower values suppress vertical flow and increase lateral discharge. The net effect on regional oil migration is likely to be small, given the small changes imposed on flow rates and patterns. The coupled effect on heat transport, however, can be more important as even modest increases in vertical flow can have a pronounced effect on heat flow (fig. 15).

Several other factors affect regional groundwater flow and heat transport in sedimentary basins, but space does not permit for the display of the multiple permutations and combinations of parameter ranges plausible in this model for the Western Canada basin. Garven and Freeze (1984a, b) illustrate a full spectrum of simulations for other controlling factors such as basin geometry, heterogeneity in permeability, and surface topography. Even the heat flux prescribed along the base of the numerical model is unknown of course for our paleogeothermal conditions. Majorowicz and others (1985) have estimated possible ranges for basement heat flow in Alberta that can provide a range of values for the numerical model (fig. 16). In this case, changes in basal heat flow scale nearly linearly.

Despite inherent uncertainties of parameter estimation, deterministic modeling of flows in sedimentary basins provide one useful tool for comparing various mechanisms of oil migration. The hydrogeologic model presented above for the Western Canada basin is based on a geologically well-constrained stratigraphic, hydraulic, and thermal framework. The general pattern of gravity-driven groundwater flow in the basin is reasonable for Tertiary time, and this flow system more than likely played a major role in the regional transport of hydrocarbons. In the sections to follow, mass transport simulations are presented as probable scenarios for oil migration, using the hydrogeologic parameters from figure 9 as one representative case for comparison purposes.

Solute transport model.—The first transport mechanism to be evaluated involves the case of miscible migration of oil in aqueous solution (fig. 17A–F). Hydrogeologic conditions are identical to those of figure 9D and G. Mathematically characterized particles are used here to track advection and dispersion of soluble hydrocarbons entering the Upper Devonian aquifer in the recharge part of the basin. A cluster of particles is released at a point (denoted with the diamond symbol in fig. 17) in the upstream end of the flow system, and it disperses into a cloud as the particles are entrained into the aquifer. The point of release is purely a

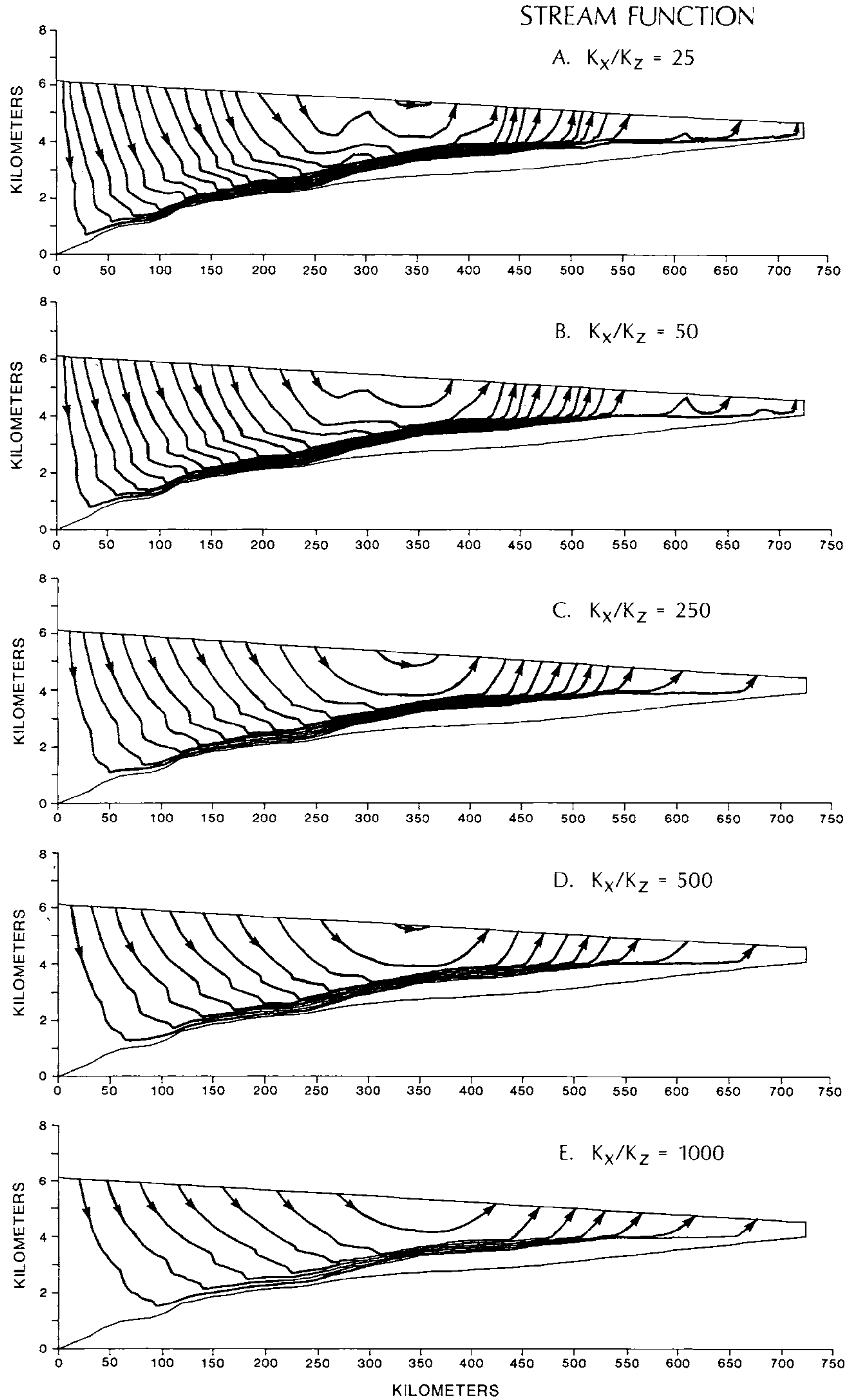

Fig. 14. Effect of basin-scale anisotropy in hydraulic conductivity on groundwater flow. Streamline contour interval is 50 m^2/yr.

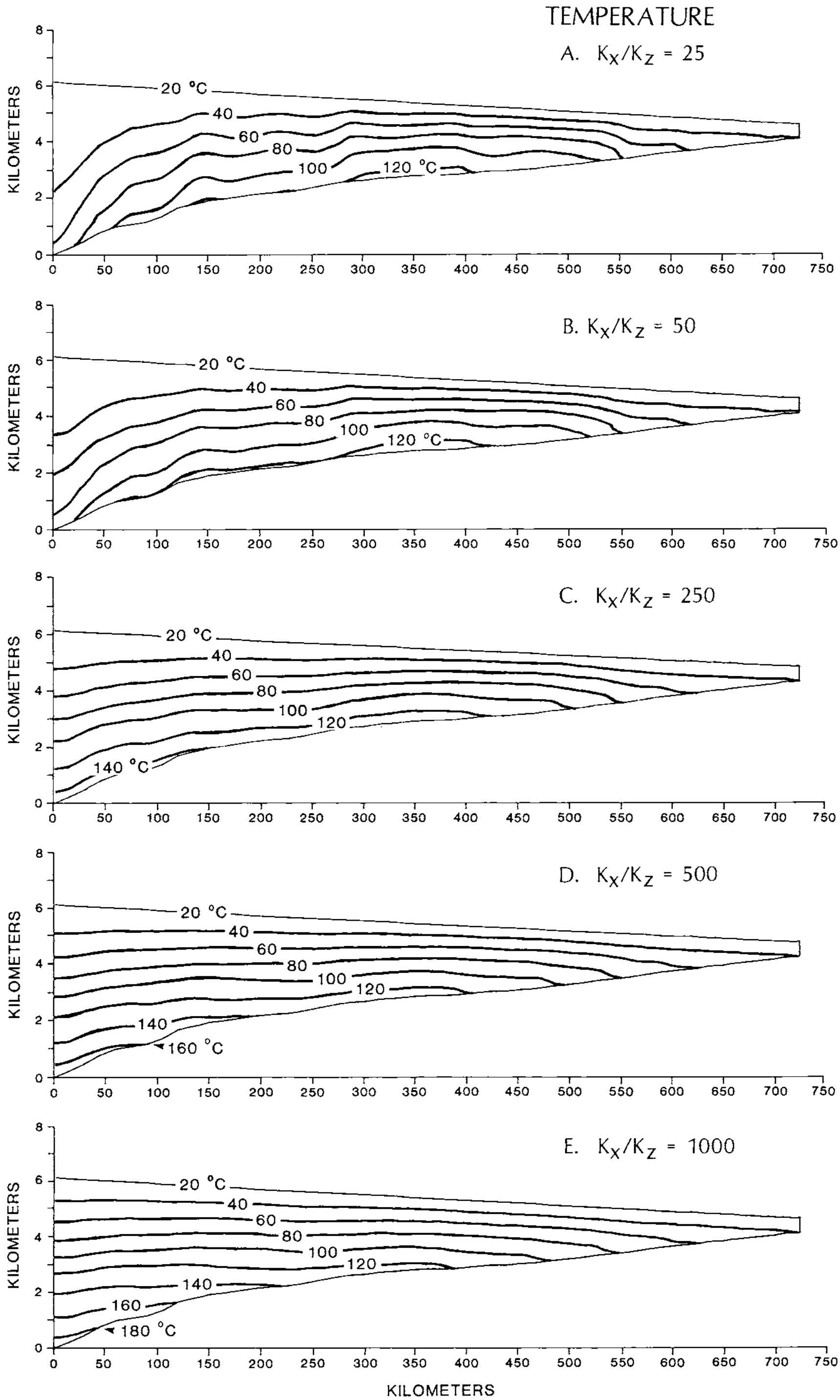

Fig. 15. Effect of basin-scale anisotropy in hydraulic conductivity on heat flow. A heat flux of 70 mW/m^2 is applied along the basement in all simulations.

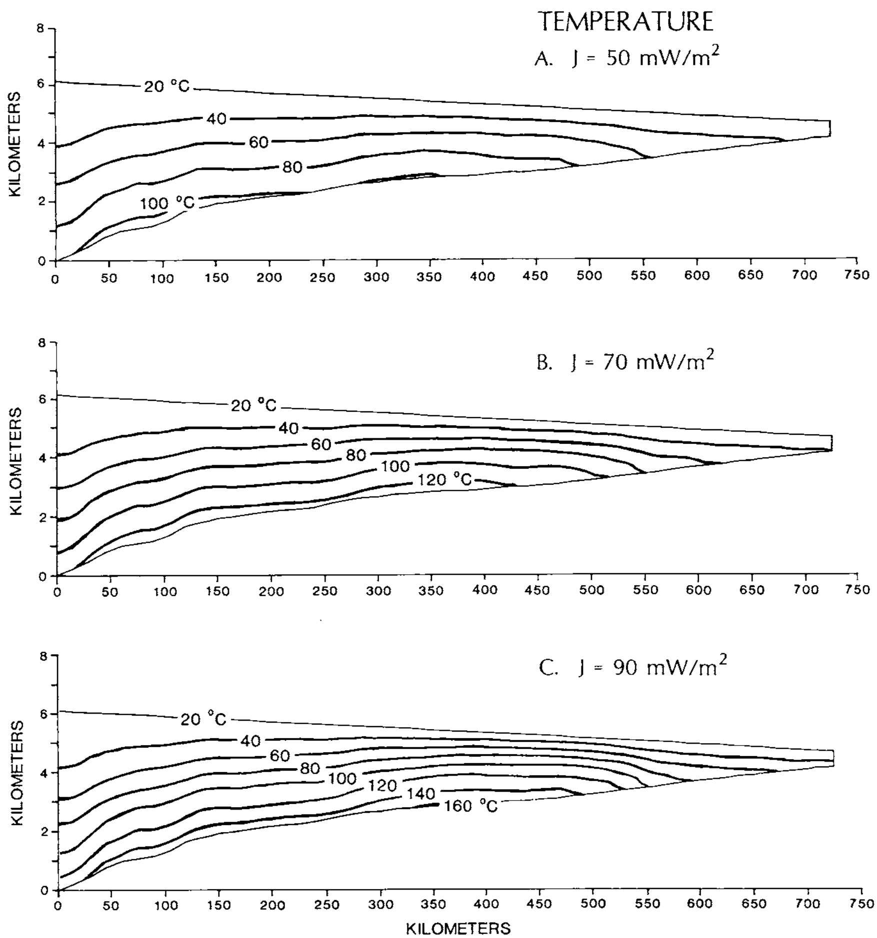

Fig. 16. Effect of basement heat flux on temperature in the western Canada basin model.

mathematical device, but it serves to mark hydrostratigraphic unit 5 (Banff and Exshaw Formations) as one possible source bed. A more detailed simulation would have particles released from numerous locations all along the inflow side of the Upper Denovian aquifer, since dissolution of hydrocarbons could occur from any of the overlying strata within the "oil window" of descending flow (fig. 9G, H). Based on figure 9H, all the Mississippian to Jurassic strata and parts of the Lower Cretaceous could have acted as potential source rock for hydrocarbon generation and therefore subjected to dissolution by descending groundwater. The transient evolution of the dispersing particle cloud

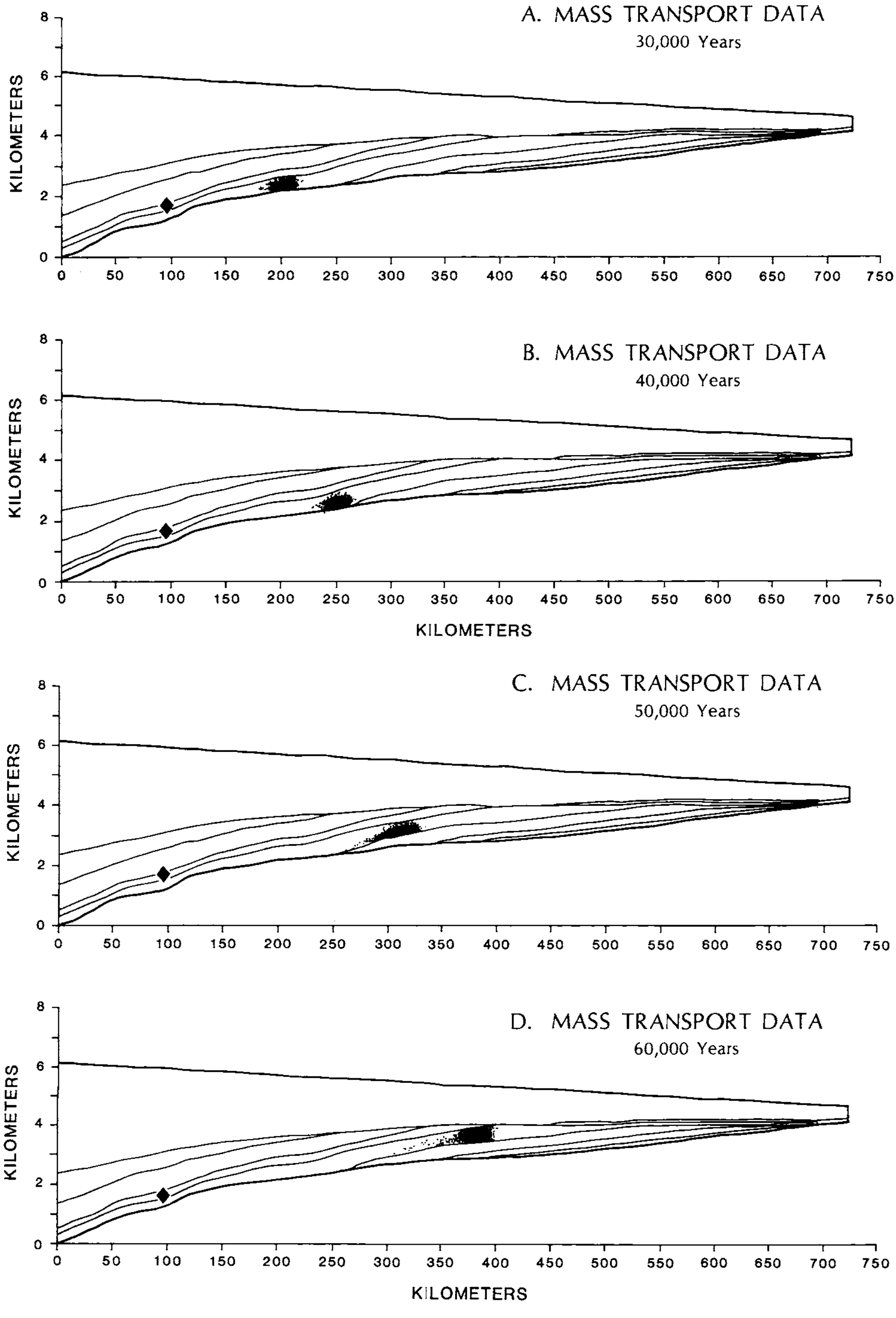

Fig. 17. Solute transport model for long-distance miscible transport of hydrocarbons in the Upper Devonian aquifer. The diamond symbol marks the point of introduction of mathematical particles used to track soluble hydrocarbons in the groundwater system.

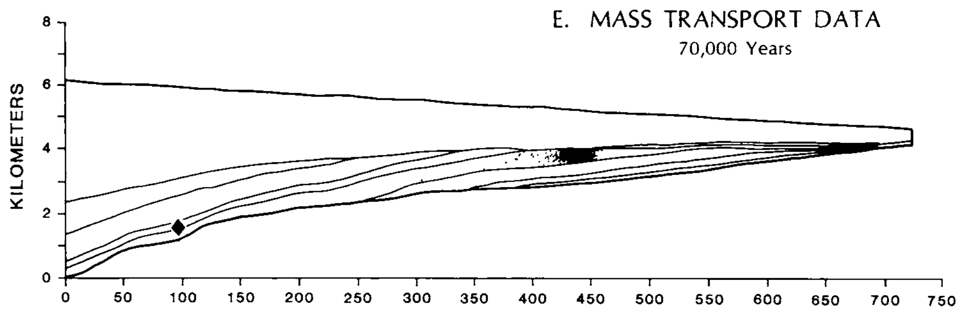

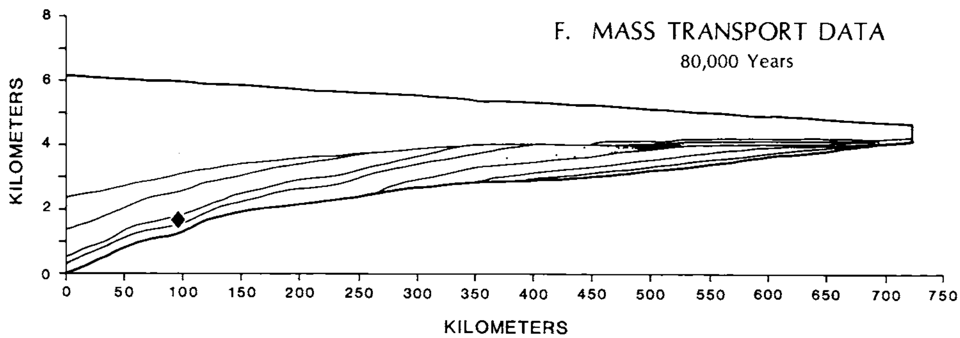

Fig. 17. (continued)

(fig. 17A to F) demonstrates the probable paths and rates of mass transport for oil generated deep within the basin. Based on the sensitivity results given earlier, this general transport pattern for soluble oil migration would hold over a wide range of aquifer/aquitard permeability situations, although the specific rates of oil transport would scale near linearly with the hydraulic conductivity of the Upper Devonian aquifer. No attempt has been made at this stage to incorporate the geochemistry of oil dissolution, precipitation, or biodegradation into the transport model, because so little is known about the thermodynamics and speciation of hydrocarbons in basinal brines (Shock, 1987). Nevertheless, it is clear from the hydrodynamic model that large parts of the Middle to Upper Devonian and Cretaceous are unlikely contributors of soluble oil for the formation of the giant oil sands deposits. A fluid particle entering the foreland would descend across the low permeability Cretaceous-Mississippian strata acquiring salinity and hydrocarbons with depth. Particle temperature would rise along the flow path from 20°C at the water table to about 120°C near the top of the Upper Devonian aquifer. Once in the aquifer, the particle would travel laterally across the basin in a near isothermal state until discharging into the Mannville sands (fig. 18).

Fig. 18. Traces of the fluid particle temperature and pressure along the transport path shown in figure 17.

Separate-phase transport model.—The second transport mechanism to be investigated involves the case of immiscible oil migration in separate-phase (fig. 19A–F). As in the previous case, numerous migration scenarios can be investigated with the numerical model. Once again a set of mathematical particles are released from a specified source area in order to track the path and rate of regional migration. Transport of separate-phase oil is driven by both the impelling force of the groundwater flow and the body force of buoyancy (fig. 9F). Oil released at a source bed (denoted by the diamond symbol) within the lower part of the Upper Devonian aquifer (fig. 19A) slowly rises to the top of the aquifer, where it is forced to pool due to the extensive, low permeability Mississippian strata which act as a barrier for upward oil migration. The oil slug migrates over 100 km laterally after 50,000 yrs of groundwater flow (fig. 19B) and over 400 km after 150,000 yrs of transport (fig. 19F) where it reaches the Mannville sands. The viscosity and buoyancy effects cause the oil slug to migrate at a rate less than half that of oil in solution. A model allowing for temperature corrections to oil viscosity might predict a slower rate of petroleum migration as the oil becomes more viscous along its flow path (Levorsen, 1967, p. 547). The temperature at the top of the Upper Devonian aquifer (fig. 9H) ranges between 120°C at the deepest part of the basin to 80°C just inside the Mannville sand unit, with the cooling rate comparable to that shown in figure 18. Oil viscosity would increase from about 2×10^{-3} to 3×10^{-3} Pa·s over this temperature range (Streeter and Wylie, 1975, p. 717). Therefore, transport times for separate-phase oil migration could be as much as three times those for aqueous transport because of viscosity effects alone.

Scenarios of buoyancy-driven oil migration restrict the possible source rocks contributing to accumulation in the Mannville sands to strata either within the Upper Devonian aquifer (Wabamun, Winterburn, Woodbend, Grosmont Formations) or immediately below it (Duvernay, Ireton, Beaverhill Lake Formations). Oil generated in the Mississippian to Lower Cretaceous sediments would appear to have little opportunity to enter the Upper Devonian aquifer under separate-phase flow, given the hydrodynamic pattern and buoyancy forces depicted in figure 9F. Oil generated within the Lower Mississippian section (Exshaw and Banff Formations) could migrate literally and upward toward the sub-Cretaceous unconformity, most likely along the Mississippian-Permian unconformity surface (fig. 20). The transport rates shown here are slower because of the lower hydraulic conductivity assumed for the rocks comprising hydrostatigraphic unit 6 (table 4). Fluid migration under this scenario would result in accumulation of the oil sands deposit in the Peace River area (Vigrass, 1968; du Rouchet, 1985).

V. *Discussion of Results*

Post-Laramide uplift of the Western Canada sedimentary basin triggered the creation of a topography-driven hydrodynamic system capable of transporting large volumes of groundwater across the foreland platform. This flow system provided the necessary mechanism for transporting and accumulating the immense amount of oil preserved today in the Mannville Group sands at the eastern edge of the basin. The modeling simulations show the ability of the Upper Devonian carbonates to act as a regional aquifer in focusing groundwater flows on the order of 10^3 to 10^4 m^3/yr (per meter width) across the Mesozoic and Late Paleozoic shale sequence in the foreland, which provided a source of soluble hydrocarbons. Maximum groundwater flow rates of 1 to 20 m/yr could have been generated in the regional aquifer, just beneath the Mannville sand reservoir. Regional groundwater flow would have had a major influence on heat flow in the basin, possibly providing nearly isothermal conditions for transport in the Upper Devonian aquifer.

In the soluble-phase transport model, hydrocarbons formed during subsidence of the foreland bulge were later dissolved in small quantities by the newly created regional flow which transported oil updip to the discharge end of the flow system. Figure 21 summarizes the parameter sensitivity study (fig. 10) and gives mass balance calculations estimating the duration of solute transport required to account for the known volume of oil in place at the Athabasca deposit, assuming a plausible range of oil concentration. For example, a flow rate of 1 m/yr with oil concentration change of 20 ppm would require 50 million years of transport, while a flow rate of 20 m/yr with 5 ppm oil would only require 10 million years.

The cause of oil precipitation or deposition in the Mannville sands is unknown, but the concentration effect of converging flow lines (fig. 9G) and change in temperature (fig. 9G, J) could have played major roles. Changes in groundwater salinity could provide an additional explanation (Vigrass, 1968). A similar scenario of thermally-controlled deposition from solution was proposed by Wood and Hewett (1984) and

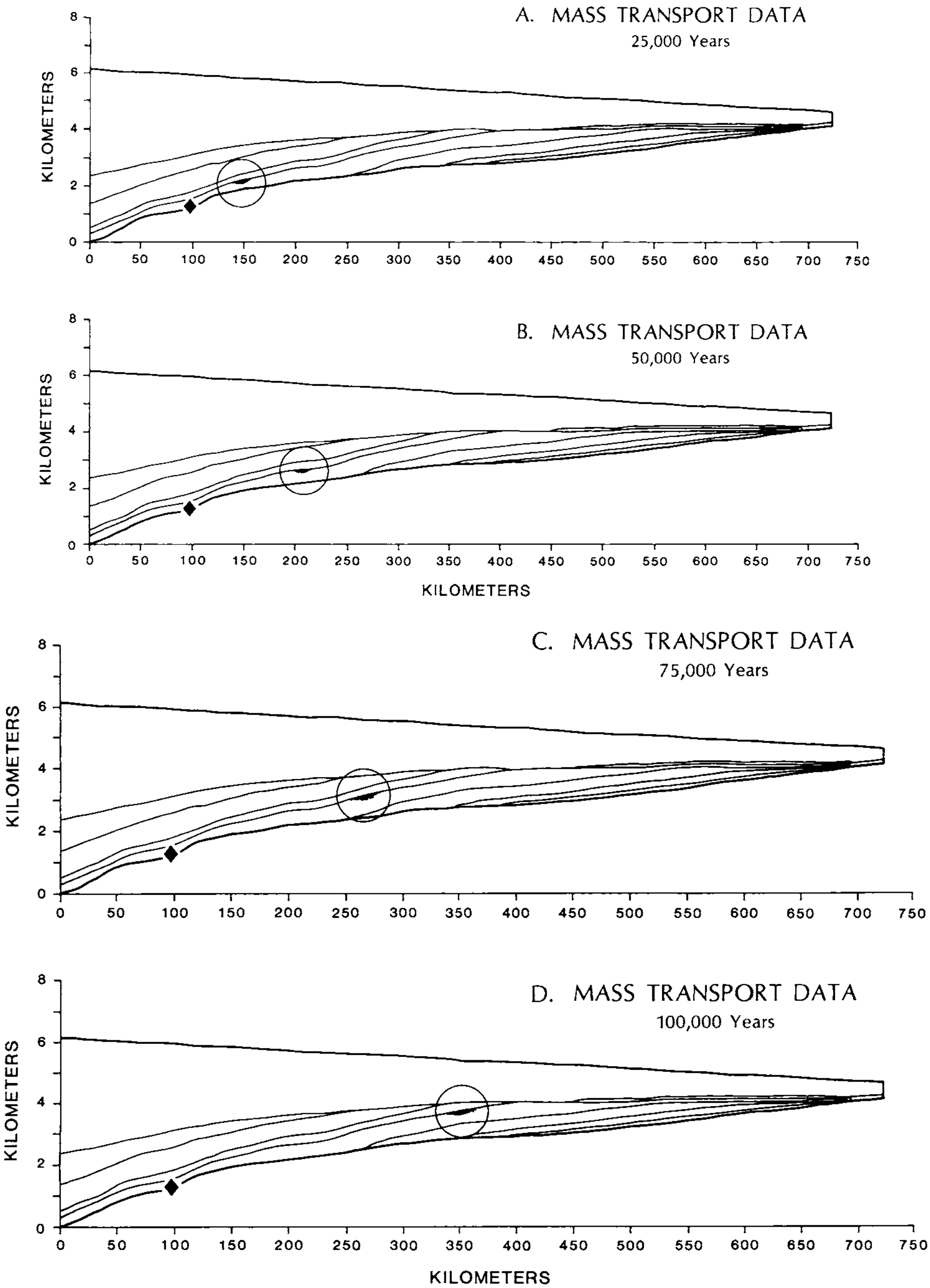

Fig. 19. Separate-phase transport model for long-distance immiscible transport of hydrocarbons in the Upper Devonian aquifer. Buoyancy forces cause the free oil to hug the top surface of the aquifer and pool in the Mannville sand unit at the basin margin. The oil phase has a constant density of 850 kg/m^3 and viscosity of 2×10^3 Pa · s.

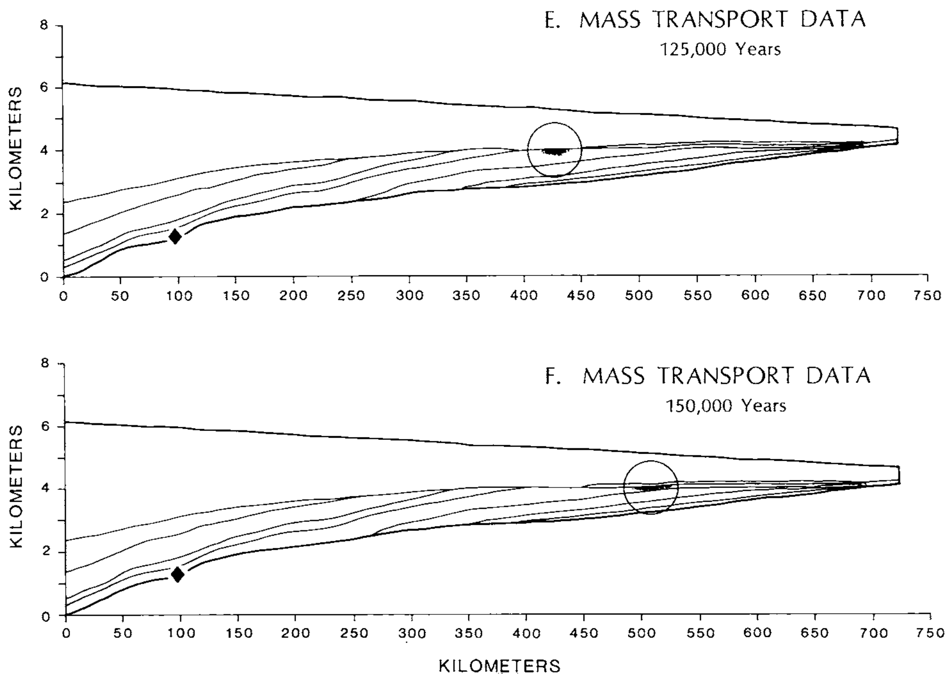

Fig. 19. (continued)

by Rabinowicz and others (1984). Two problems exist in a thermally-controlled precipitation model. Firstly, the rate of oil deposition may be small if the solubility-temperature curves of Price (1976) are indicative of aqueous transport of hydrocarbons in the Alberta basin. However, large quantities of brines have traversed the sub-Cretaceous unconformity, and with gravity-driven flow there is little problem in satisfying mass balance constraints (fig. 21). It is also likely that temperature changes were not solely responsible for oil deposition, as equilibrium conditions could just as easily been perturbed by other changes in fluid or rock composition. Secondly, with the known temperature effect of oil solubility (fig. 8), one might also expect the molecular composition of exsolved hydrocarbons to be of similar type as the source phase (McAuliffe, 1980; Wood and Hewett, 1984). However, this may be a premature conclusion given our limited understanding of the aqueous geochemistry of petroleum and of the effects of biodegradation in a basinal-brine environment.

In the separate-phase transport model, hydrocarbons formed during early subsidence would migrate under the forces of buoyancy and capillarity up into more permeable lithologic units. Most of this primary migration would probably occur through fracture networks (Palciauskas

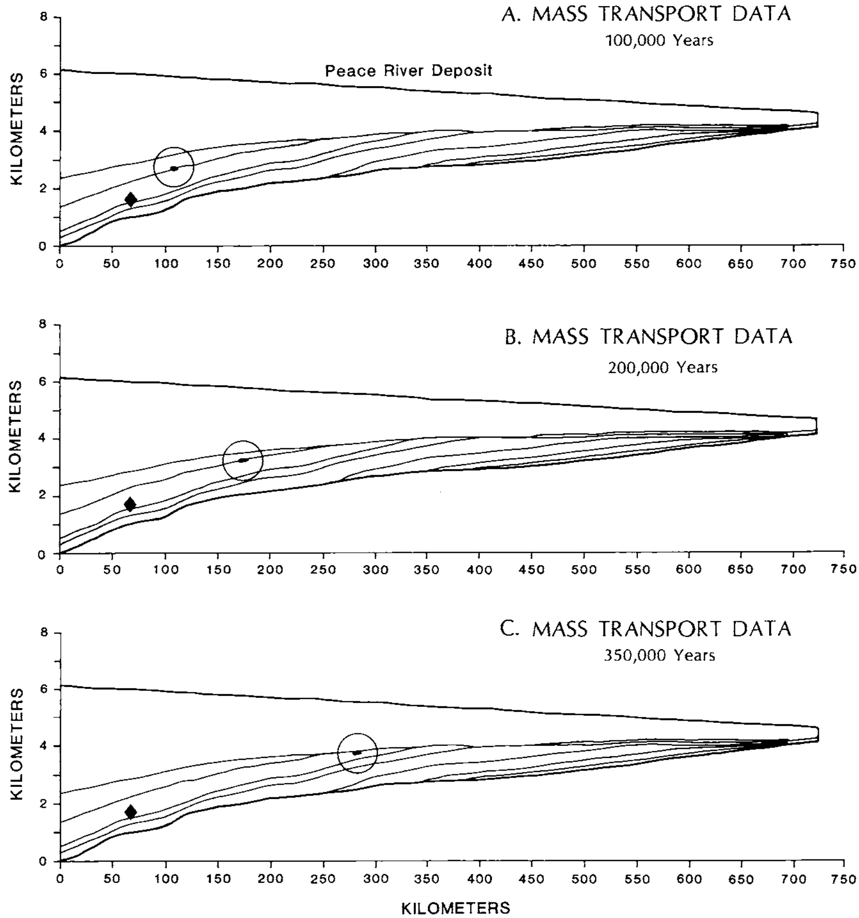

Fig. 20. Separate-phase transport model for immiscible transport of hydrocarbons in the Mississippian-Permian hydrostratigraphic unit. Oil generated within the lower Mississippian as a separate-phase would be partly dissolved by descending groundwater, with the remaining volume migrating updip and accumulating in the Peace River deposit.

and Domenico, 1980; du Rochet, 1981; Magara, 1981; Ozkaya, 1988). With the advent of the topography-driven flow system, immiscible oil slugs could be driven laterally across the basin, primarily along the tops of regional aquifers. One simulation demonstrates the possibility for oil to migrate out of Devonian shale up into the Upper Devonian aquifer, where it is driven toward the Mannville sands but at a rate two to three times slower than that of oil in aqueous solution. The Mississippian through Lower Cretaceous section is another possible source of hydrocarbons, but it is difficult to conceive of a separate-phase flow mechanism that could transport oil downward into the Upper Devonian

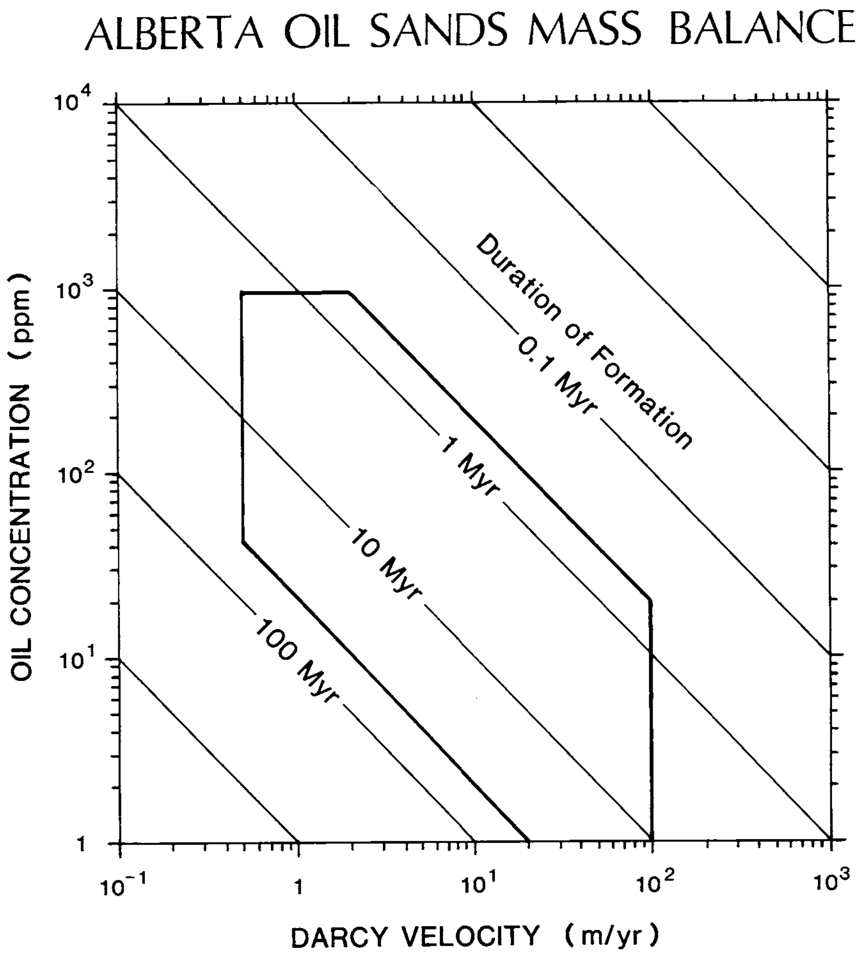

Fig. 21. Mass balance diagram summarizing possible scenarios of Darcy flow rates and oil concentration in basinal brines for the Athabasca oil deposit (oil in place ~ 1.4×10^{11} m^3). The calculations assume an effective flow area swath of 320 km wide by the thickness of the Upper Devonian aquifer. The region boxed-in by the thick line represents geologically reasonable parameter ranges for topography-driven flow.

aquifer. A more likely situation for the post-Devonian rocks is the upward flow of hydrocarbons into thinner Mississippian and Triassic aquifer zones associated with unconformities. Regional groundwater flow would then drive the free oil updip toward the sub-Cretaceous unconformity with accumulation in the Peace River area (fig. 20). Upward migration of oil globules in the Mississippian to Lower Cretaceous section would also provide abundant opportunity for extensive dissolution of hydrocarbons by the descending groundwater flow, and so the actions of both transport mechanisms could be complementary.

The relative timing and fraction contribution by separate-phase transport to overall accumulation in the oil sands deposits are somewhat speculative due to uncertainties in the rate of hydrocarbon generation and primary migration. Massive and continuous oil-phase migration is unlikely to have been widespread because of the low organic content (0.5–2.0 percent) of most of the potential source rocks in the Western Canada basin (Deroo and others, 1977; Moshier and Waples, 1985). Exceptions to this generalization, however, include the thin Devonian Duvernay and Jurassic Nordegg shales (fig. 6) which may contain up to several wt percent organic carbon. Upper Devonian shale of the Beaverhill Lake, Duvernay, and Ireton Formations are juxtaposed to contribute the most oil for the Grosmont-Athabasca deposits through separate-phase migration, based on the hydrodynamic pattern of petroleum (fig. 9F) and the thermal profile (fig. 9H). Potential petroleum flow rates on the order of 10^{-3} $m^3/m^2 \cdot yr$ are predicted for the source beds below the Upper Devonian aquifer, but these calculations do not account for the effects of capillarity. Indeed, the numerical model computed flow rates for the basin shales three to four orders of magnitude higher than the rate of oil generation thought to occur in shales (England and others, 1987). Better model calculations would clearly require that effects of capillarity be included for simulating primary oil migration in the shale source rocks.

The total generative capacity of the Devonian shale section can be estimated, knowing the organic-carbon content, the oil-generative capability of the kerogen, and the thermal maturation achieved by the organic matter (Moshier and Waples, 1985). Assuming a 200 m average thickness over a source area of 300 km by 300 km gives a total rock volume of 1.8×10^{13} m^3. Using a total organic carbon content average of about 0.5 percent, a hydrocarbon-generative capacity of kerogen of 0.1 kg/kg of organic carbon (Deroo and others, 1977) and a fractional conversion of 50 percent result in a maximum of 10^{10} m^3 of oil generated from the Upper Devonian shales, about one-tenth of the estimated volume of oil in the Athabasca deposit. A similar contribution from the Upper Devonian carbonate aquifer itself given twice the area and half the organic content could double the possible source capability. Therefore, separate-phase oil migration from the Upper Devonian alone is capable of explaining only a fraction of the oil preserved in the Mannville sands.

COMMENTS ON THE ROLE OF TRANSIENT FLOW

The Western Canada sedimentary basin underwent two major periods of subsidence during its tectonic evolution (Bally, Gordy, and Stewart, 1966; Porter, Price, McCrossan, 1982; and Beaumont and others, 1985). The earliest period occurred in the Late Precambrian to Paleozoic when the basin developed as a continental shelf and platform of a passive margin extending to the west. The Permian to Middle Jurassic wedge of multiple unconformities (fig. 2) represents the closing stages of this phase. The latest period of subsidence is recorded as a series of shale and molasse sediments derived from overthrust sheets which formed during the accretion of allochthonous terranes onto the western margin of North America. This period of compression and thrusting was most active in the Cretaceous through Eocene time with culmination of the Laramide orogeny. Beaumont (1981) describes the foreland subsidence as the result of flexural downwarping of the lithosphere due to the loading of the crust by overthrust sheets to the west. Following the Laramide orogeny, flexural relaxation of the lithosphere resulted, because erosion of the mountain belt removed part of the original load. Subaerial erosion, interrupted briefly by continental glaciations in the Pleistocene, is still continuing to the present time.

The tectonic history of the foreland and platform provides a reasonable framework for conceptualizing the hydrologic evolution of the Western Canada basin (fig. 22). In the Late Paleozoic, compaction of marine sediments provided the sole mechanism for driving fluid flow in the subsiding basin (Bredehoeft and Hanshaw, 1968). The exact flow patterns and rates are unknown for this stage, but it is likely the flows

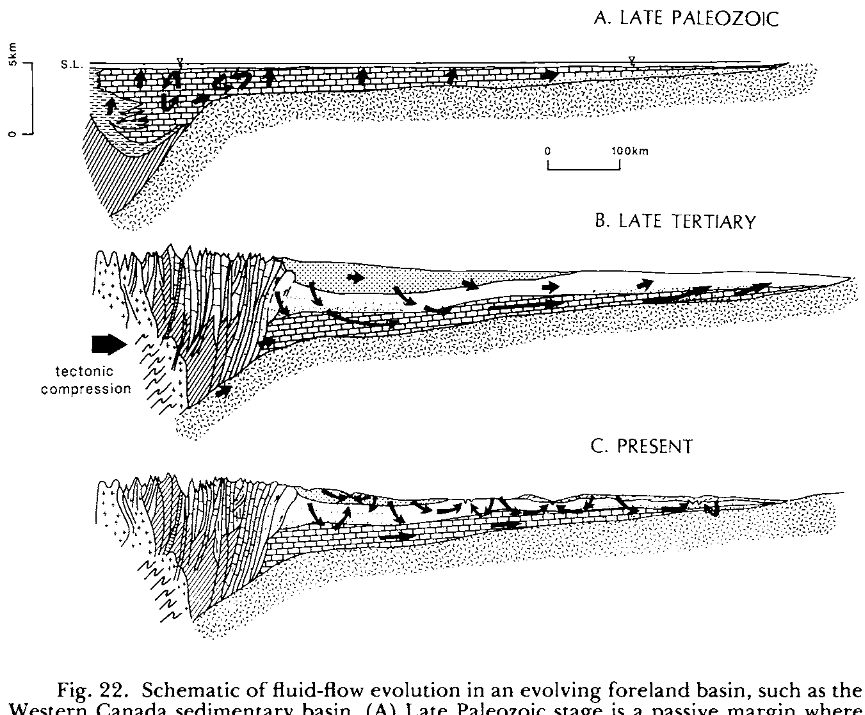

Fig. 22. Schematic of fluid-flow evolution in an evolving foreland basin, such as the Western Canada sedimentary basin. (A) Late Paleozoic stage is a passive margin where flow is dominated by thermally-driven convection and compaction. (B) Late Tertiary stage represents the period soon after tectonic compression and flexural uplift. Gravity-driven flow dominates with regional migration of brines and hydrocarbons. (C) Present-day fluid flow pattern is strongly partitioned and weakened by erosion of topography.

were dominantly upward at maximum rates of 10^{-3} m/yr or less, based on theoretical calculations of compaction in sedimentary basins (Sharp, 1978; Bethke, 1985; Shi and Wang, 1985). A more important mechanism of mass transfer in this period of basin evolution may have been the convective circulation of thermally-driven flow. Figure 23A and B show one simulation example of paleoflow in the Western Canada basin prior to the Laramide orogeny, with the same hydraulic properties of table 4. Groundwater circulates more vigorously in the thicker part of the basin and across several stratigraphic units, but most of the fluid flow is confined to the Upper Devonian aquifer where Darcy velocities reach a maximum of 10^{-2} m/yr. Vertical flow rates are smaller, yet sufficient enough to perturb the geothermal gradients in the shelf region (fig. 23B). However, only a small part of the basin is exposed to fluid flow, and no regional mechanism exists for transporting large volumes of basinal brines or hydrocarbons to the eastern margin.

Tectonic compression and thrusting during Mesozoic time would have initiated a second-phase of compaction-driven flow from the orogenic belt, possibly in the manner hypothesized by Oliver (1986) with focusing of fluid flow in front of thrust sheets. The effect of compression and thrusting on the hydrodynamics of foreland basins has just begun to be quantified. Bethke (1986b) estimated maximum flow

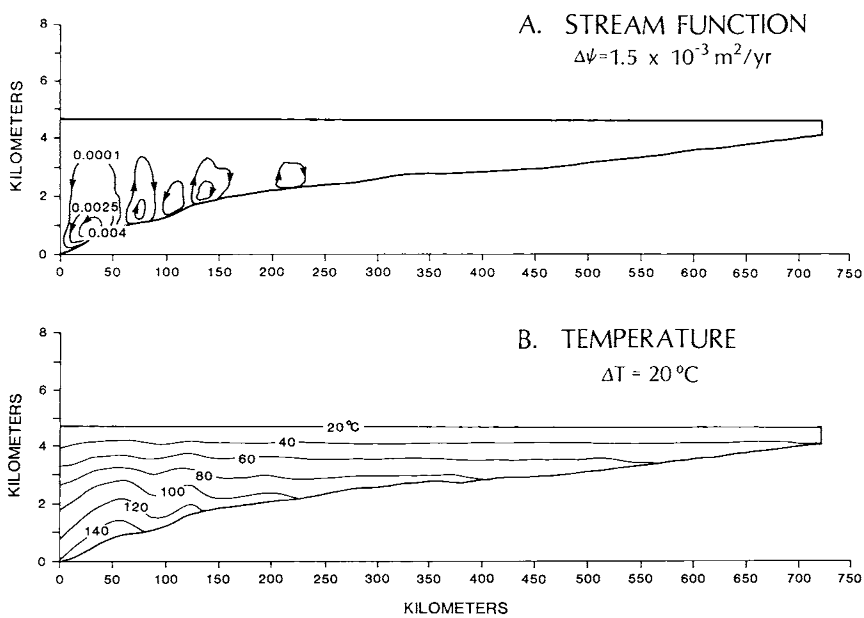

Fig. 23. Hydrogeologic model of steady-state flow in a compacted margin and continental platform. Fluid flow is solely driven by density gradients.

rates of only 10^{-2} m/yr based on rates of crustal plate convergence, whereas Ge and Garven (in press) have computed transient flow rates of 10^{-3} to 10^{-2} m/yr based on coupled stress–strain–flow models of a foreland thrust. Despite the low groundwater flow rates, this stage of basin subsidence and compression was perhaps the most conducive for oil maturation because of the depth of burial in the foreland wedge (Beaumont and others, 1985). It is possible that this stage in basin development also enhanced primary migration of hydrocarbons down into the Devonian aquifers so that later solution and separate-phase oil was driven updip by gravity-driven flow. The volume of hydrocarbons driven by compression and compaction is likely to have been small, however, in light of the flow calculations by Ge and Garven (in press).

Subsequent uplift and erosion of the Rocky Mountain fold and thrust belt resulted in widespread emergence of the basin foreland and platform and the creation of a topography-driven flow system (fig. 22B). Figures 24 and 25 show the transient evolution of fluid flow and heat transport predicted with the numerical model, assuming an instantaneous regression of the Cretaceous-Tertiary seaway with basin uplift. Both the hydraulic and thermal systems evolve to a steady pattern after 1 million years of flow, although the temperature field requires a longer period of dissipation because the thermal diffusivity coefficient is two orders of magnitude smaller than the hydraulic coefficient in the transport equations (table 2). Fluids traversing the basin soon after uplift would be initially cool in the regional discharge area and later heat up due to the effect of forced convection. Figure 26 documents the detailed transitions of the fluid velocity and temperature for a single point in the Upper Devonian aquifer at $x = 500$ km (fig. 9A), which is in the discharge end of the flow system and directly below the Mannville sand reservoir. The horizontal component of the Darcy velocity rises to a steady value of 1.6 m/yr after only 1000 yrs of flow, while the vertical component takes a period of 100,000 yrs to reach steady state. Variations in the vertical velocity component result from buoyancy-driven transients associated with the evolving temperature field and from vertical heterogeneities in the permeability field. This effect on the vertical velocity component feeds back into the energy equation through the convection terms in eq (6), which in turn have a pronounced effect on the temperature of the fluid discharging into the Mannville sands (fig. 26B). The magnitude of the observed thermal pulse directly varies with the aquifer hydraulic conductivity. For example, a hydraulic conductivity of 800 m/yr produces a thermal pulse of similar duration as the case for 200 m/yr (fig. 26B), but fluid temperatures climb to 150°C in the regional discharge area (Garven, 1988). The marked variation in temperature between 100,000 and 200,000 yrs (fig. 27) could help explain the range in fluid-inclusion temperatures observed in hydrothermal minerals associated with base-metal ores (Sverjensky, 1986). The role of fluid transients in oil migration is unclear. J.R. Wood (personal commun.) has offered the suggestion that thermal transients

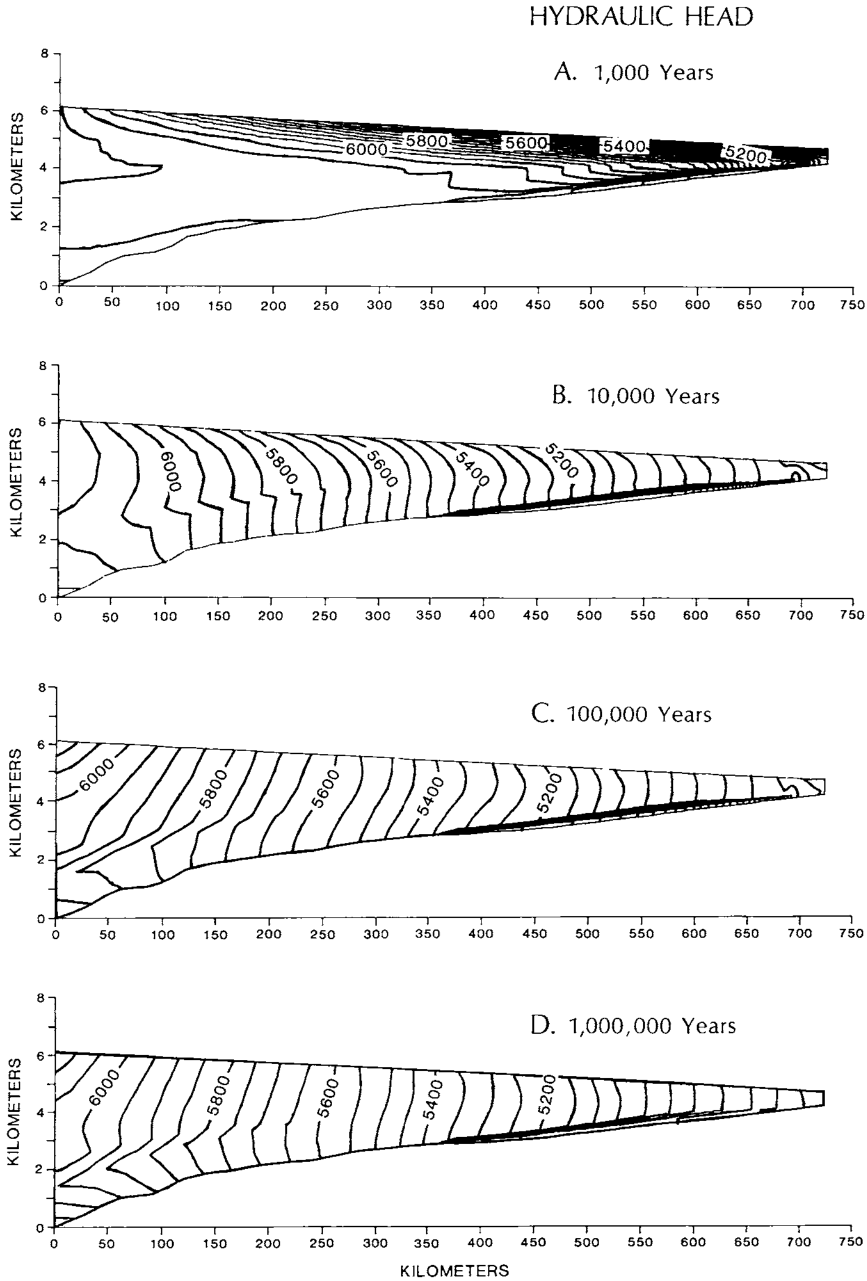

Fig. 24. Transient groundwater flow model showing the evolution of hydraulic heads for an instantaneous withdrawal of epeiric seas from the Tertiary foreland basin.

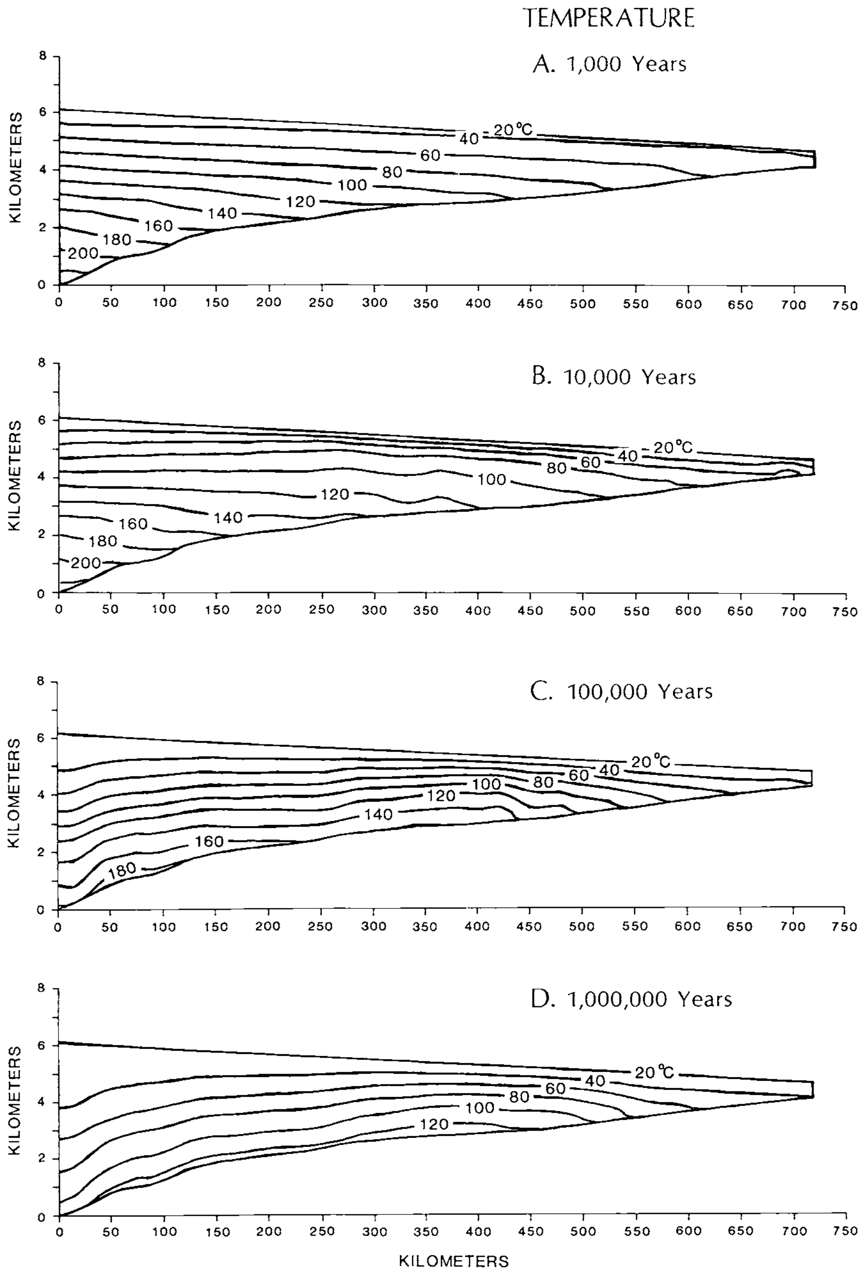

Fig. 25. Transient heat flow model showing the evolution of temperature for the companion hydraulic fields of figure 24.

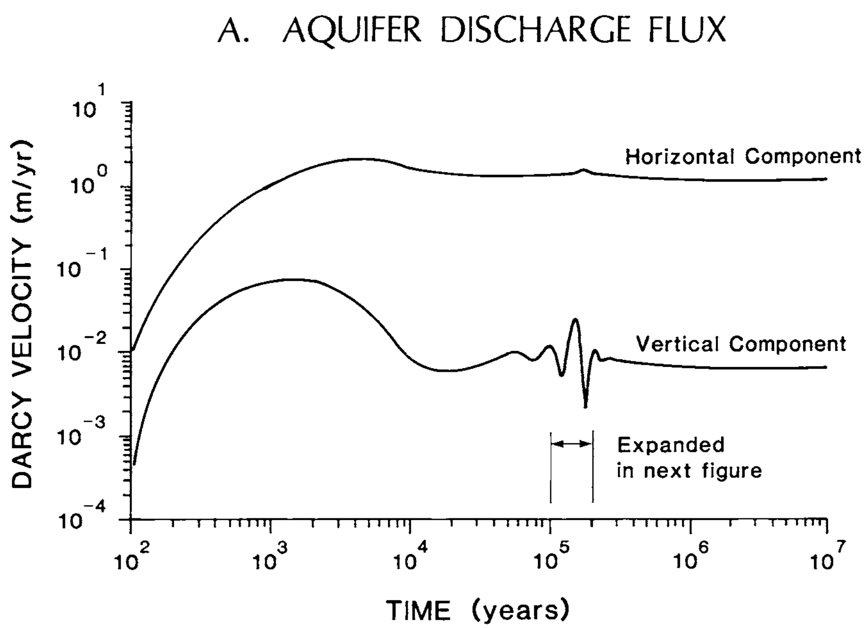

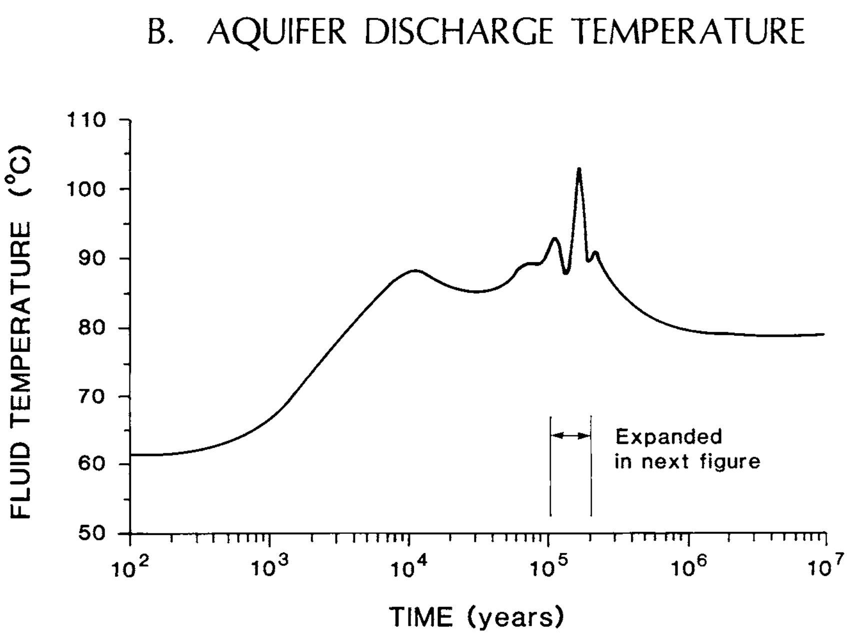

Fig. 26. Fluid temperatures and flow rates as a function of time in the discharge area near the sub-Cretaceous unconformity (fig. 9G).

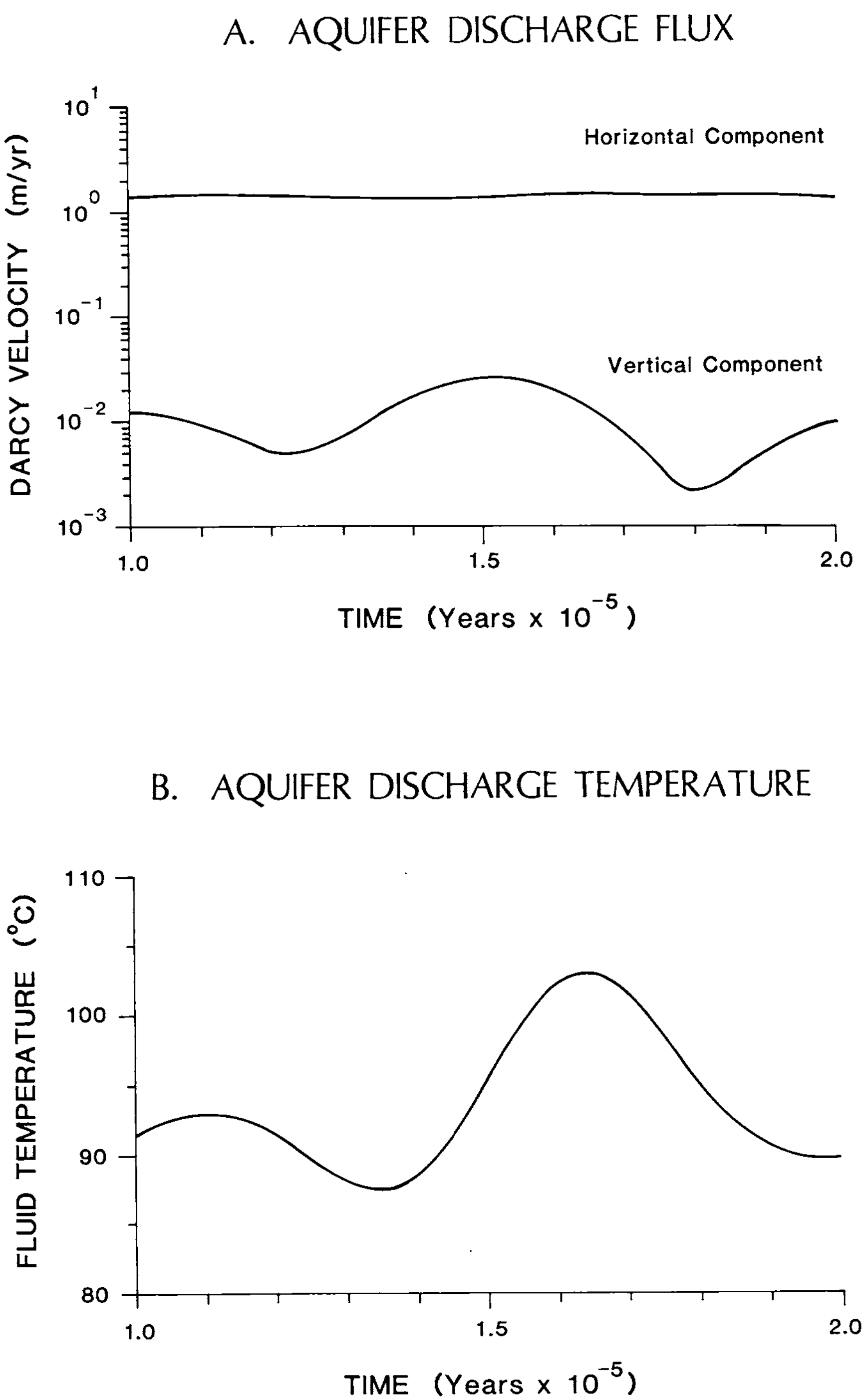

Fig. 27. Expanded view of the temporal changes in flow rates and temperature in figure 26.

induced by flow may help explain organic maturation anomalies observed in certain intracratonic basins such as the Michigan basin (Cercone, 1984; Vugrinovich, 1988). The thermal transients illustrated in figure 25 could have a profound effect on the organic maturation of sediments as the pulse traverses the basin.

Based on the tectonic history of the basin, the gravity-driven flow system could have operated for as long as 50 million years, transporting hydrocarbon-bearing groundwater and impelling separate-phase oil through the Upper Devonian aquifer with deposition and pooling in the Mannville Group sands. Separate-phase oil probably migrated upward into the regional aquifer from underlying Devonian shale, but a large percentage of the giant oil sands accumulation must have resulted from soluble transport of hydrocarbons generated within Mississippian to Cretaceous strata in the foreland bulge at the recharge end of the flow system. Concentration effects may have forced a lot of oil in solution to form a separate phase along the updip portion of the aquifer, such that most of the oil arrived as an immiscible fraction at the sub-Cretaceous unconformity. By Late Pliocene time, differential erosion developed an incised surface drainage system that dissipated the regional flow into local flow systems (fig. 22C). Numerical simulations of the present-basin configuration suggest flow rates of 1 m/yr in the most permeable aquifers and a temperature field that is a subdued relict of mid-Tertiary

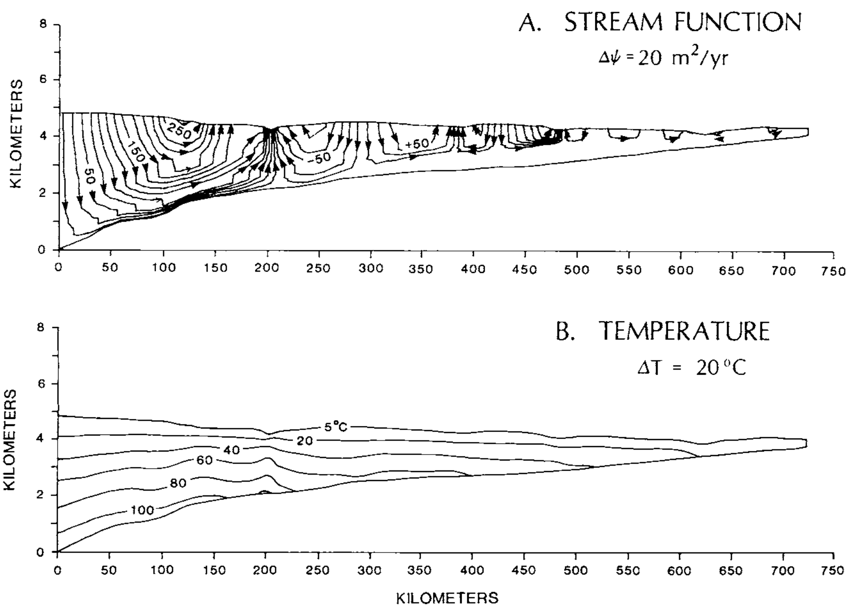

Fig. 28. Hydrogeologic model of steady-state fluid and heat flow fields for the western Canada basin in Holocene time.

time (fig. 28). The Holocene groundwater flow is more than adequate for redistributing petroleum as documented by Tóth (1980), although the regional mechanism originally present for transporting large volumes of oil toward the basin margin no longer existed. The development of local flow systems represented a period of biodegradation and dissolution of the oil sands deposits by shallow-circulating groundwater.

CONCLUSION

The Western Canada sedimentary basin provides an excellent example of the close relationship between tectonics, hydrogeology, and the formation of large oil and ore deposits in foreland basins. Compression and thrusting along the western margin of the continent eventually led to flexural uplift of the foreland and platform in post-Cretaceous time. As a result of uplift, a gravity-driven groundwater flow system was created that focused fluids across the basin through the Upper Devonian carbonate aquifer, with upward discharge rates of 1 to 10 m/yr across the Mannville Group reservoir sands at the eastern margin. The supergiant oil sands deposits formed as a direct result of the Tertiary-age flow system. Hydrogeologic and mass balance considerations suggest that at least 80 percent of the accumulated oil was transported in solution from Mississippian to Cretaceous source rocks located within the foreland wedge. Miscible transport could have formed the giant oil sands deposits in less than 50 million years, assuming concentrations on the order of 10 ppm and precipitation caused by cooling and concentration effects in the discharge area. Separate-phase, immiscible oil transport as globules and slugs could have contributed a maximum of about 20 percent of the accumulated oil volume, but only from the Upper Devonian strata. Separate-phase migrations in the Mississippian to Cretaceous section are more likely to have formed the Peace River deposit because of buoyancy effects than to have contributed directly to the massive deposits near the edge of the basin. Transport and accumulation of large oil volumes waned in Pliocene time, due to the dissipation and partitioning of the regional flow system by erosion.

ACKNOWLEDGMENTS

I am indebted to Laurence Vigrass for sharing his expertise on the geology of the oil sands deposits and the Western Canada sedimentary basin while he visited Johns Hopkins University during a 1985–1986 sabbatical. Mark Person helped the author formulate the numerical algorithm for petroleum migration. Discussions on the origin of oil with Everett Shock, Dimitri Sverjensky, and Jim Wood benefitted the development of the research. Chris Neuzil provided much insight on the transient nature of groundwater flow in sedimentary basins, and Edward Bouwer supplied useful information on the effects of biodegradation of hydrocarbons in the subsurface. Hugh Ellis contributed thoughtful comments for improving an early draft of the manuscript. The author is also grateful to Antonio Lasaga and Carl Steefel for their perceptive reviews.

The work reported in this paper was supported by grants from Conoco Inc. and the National Science Foundation (EAR-8409609). Computational support was provided through equipment grants from Texaco, Inc. and the National Science Foundation (EAR-8553019).

Appendix

Numerical formulation of the transport equations

The models of regional groundwater flow and oil migration are based on numerical simulations with the hybrid finite element and particle tracking code OILGEN, which was developed for this study. Because the fluid flow, stream function, and heat transport equations (table 2) are of the same form, a common numerical solution procedure was used. The irregular geometry of the basin and hydrostratigraphy (fig. 9A) makes the use of the finite element method most suitable. As a first step in the procedure, the flow domain is discretized into a set of triangular elements defined by nodal coordinates (fig. 9B). By assuming an unknown function $\Phi = \Phi(x, z, t)$, where Φ stands for either the head h_w, the stream function Ψ, or temperature T, we can write a trial solution for the differential equations as:

$$\Phi \sim \hat{\Phi} = \sum_{n=1}^{N} \Phi_n \xi_n(x, z) \tag{A1}$$

where N is the number of nodal points in the grid, Φ_n are the unknown coefficients, and ξ_n are linearly independent basis functions (Huyakorn and Pinder, 1983). The element basis functions are defined by

$$\xi_n(x, z) = \frac{1}{2\Delta}(a_n + b_n x + c_n z) \tag{A2}$$

where Δ is the element area and n = 1,2,3. The coefficients in (A2) are given by the local coordinates of the element nodes as:

$$\begin{aligned}
a_1 &= x_2 z_3 - x_3 z_2 \quad & b_1 &= z_2 - z_3 \quad & c_1 &= x_3 - x_2 \\
a_2 &= x_3 z_1 - x_1 z_3 \quad & b_2 &= z_3 - z_1 \quad & c_2 &= x_1 - x_3 \\
a_3 &= x_1 z_2 - x_2 z_1 \quad & b_3 &= z_1 - z_2 \quad & c_3 &= x_2 - x_1
\end{aligned}$$

and

$$2\Delta = c_2 b_1 - c_1 b_2$$

In the Galerkin finite element approach, the trial solution (interpolation formula) is substituted into the differential equation and a weighted integral over the flow domain R is formed to minimize the residual error. Eqs (3), (5), and (6) are transformed as a result of this operation to:

$$\iint_R \left\{ \nabla \cdot [\mathbf{K}\rho_w \mu_{rw}(\nabla \hat{h} + \rho_{rw}\nabla Z)] - \rho S_s \frac{\partial \hat{h}}{\partial t} \right\} \cdot \xi_n \, dR = 0 \tag{A3}$$

$$\iint_R \left\{ \nabla \cdot \left[\frac{\mathbf{K}}{|\mathbf{K}|} \mu_w \nabla \hat{\Psi} \right] + g \frac{\partial \rho_w}{\partial x} \right\} \cdot \xi_n \, dR = 0 \tag{A4}$$

$$\iint_R \left\{ \nabla \cdot [\mathbf{E}\nabla \hat{T}] - \rho_w c_w \mathbf{q}_w \cdot \nabla \hat{T} - C_B \frac{\partial \hat{T}}{\partial t} \right\} \cdot \xi_n \, dR = 0 \tag{A5}$$

for n = 1, 2, . . . , N. The specific storage coefficient in (A3) is derived for the elastic properties of the porous media as $S_s = \rho_w g(\alpha + \phi\beta)$. The bulk heat capacity in (A5) is represented by the term $C_B = [\rho_w c_w \phi + \rho_s c_s(1 - \phi)]$.

Using Green's second identity (Kreyszig, 1972) and replacing the integration over the region as a summation over the finite elements, the equations become:

$$\sum_m \left[\sum_e \int\int_{R^e} \mathbf{K}\rho_w\mu_{rw}\nabla\xi_m \cdot \nabla\xi_n \, dR^e\right] h_m + \sum_e \int\int_{R^e} \mathbf{K}\rho_w\mu_{rw}\rho_{rw}\nabla Z \cdot \nabla\xi_n \, dR^e + \sum_m \left[\sum_e \int\int_{R^e} \rho_w S_s \xi_m \xi_n \, dR^e\right] \frac{dh_m}{dt} = -\sum_e \int_{\Omega^e} \mathbf{q}_w \cdot \mathbf{n}\xi_n \, d\Omega^e \quad \text{(A6)}$$

$$\sum_m \left[\sum_e \int\int_{R^e} \frac{\mathbf{K}}{|\mathbf{K}|}\mu_w \nabla\xi_m \cdot \xi_n \, dR^e\right] \Psi_m = -\sum_e \int\int_{R^e} g\frac{\partial\rho_w}{\partial x}\xi_n \, dR^e + \sum_e \int_{\Omega^e} \frac{\mathbf{K}}{|\mathbf{K}|}\mu_w \nabla\Psi \cdot \mathbf{n}\xi_n \, d\Omega^e \quad \text{(A7)}$$

$$\sum_m \left[\sum_e \int\int_{R^e} (\mathbf{E}\nabla\xi_m \cdot \nabla\xi_n + \rho_w c_w \mathbf{q}_w \cdot \nabla\xi_m \cdot \xi_n) \, dR^e\right] T_m + \sum_m \left[\sum_e \int\int_{R^e} C_B \xi_m \xi_n\right] \frac{\partial T_m}{\partial t} = \sum_e \int_{\Omega^e} \mathbf{E}\nabla\hat{T} \cdot \mathbf{n}\xi_n \, d\Omega^e \quad \text{(A8)}$$

The integrals over the element boundaries Ω^e represent the flux or natural boundary conditions (table 3). After evaluating the integrals, eqs (A6) to (A8) can be rewritten in matrix notation:

$$A_{nm}h_m + D_{nm}\frac{dh_m}{dt} = Q_n \qquad m, n = 1, 2, \ldots, N. \quad \text{(A9)}$$

where

$$A_{nm} = \sum_e \frac{\rho_w\mu_{rw}}{4\Delta}(K_{xx}b_n b_m + K_{zz}c_n c_m)$$

$$D_{nm} = \sum_e \rho_w S_s \Delta \cdot \begin{cases} \frac{1}{6} & \text{if } n = m \\ \frac{1}{12} & \text{if } n \neq m \end{cases}$$

$$Q_n = -\sum_e \frac{\rho_w\mu_{rw}\rho_{rw}}{2}(K_{zz}c_n) - \sum_e \frac{q_n}{2}$$

and for the stream function equation

$$S_{nm}\Psi_m = B_n \qquad m, n = 1, 2, \ldots, N. \quad \text{(A10)}$$

where

$$S_{nm} = \sum_e \frac{\mu_w}{4\Delta}\left[\frac{b_n b_m}{K_{xx}} + \frac{c_n c_m}{K_{zz}}\right]$$

$$B_n = -\sum_e \frac{\rho_{wm} g b_m}{6} + \frac{B_n^{\Omega}\mu_w}{2}$$

and for the heat equation

$$R_{nm}T_m + U_{nm}\frac{dT_m}{dt} = F_n \qquad m, n = 1, 2, \ldots, N. \tag{A11}$$

where

$$R_{nm} = \sum_e \frac{1}{4\Delta}[E_{xx}b_nb_m + E_{zz}c_nc_m] + \frac{\rho_w c_w}{6}[q_x^e b_m + q_z^e c_m]$$

$$U_{nm} = \sum_e C_B\Delta \cdot \begin{cases} \dfrac{1}{6} & \text{if } n = m \\[2ex] \dfrac{1}{12} & \text{if } n \neq m \end{cases}$$

$$F_n = -\sum_e \frac{J_n}{2}$$

For steady-state problems, eqs (A9) and (A11) can be simplified by setting D_{nm} and U_{nm} equal to zero. Otherwise the time derivatives can be expanded with finite difference approximations:

$$\left[\Theta A_{nm} + \frac{1}{\Delta t}D_{nm}\right]h_m^{k+1} = Q_n - \left[(1-\Theta)A_{nm} - \frac{1}{\Delta t}D_{nm}\right]h_m^k \tag{A12}$$

and

$$\left[\Theta R_{nm} + \frac{1}{\Delta t}U_{nm}\right]T_m^{k+1} = F_n - \left[(1-\Theta)R_{nm} - \frac{1}{\Delta t}U_{nm}\right]T_m^k \tag{A13}$$

in which Θ is the time-stepping weight, and the subscript k refers to the current time level. In a fully implicit scheme $\Theta = 1.0$, and in the Crank-Nicolson scheme $\Theta = 0.5$ (Huyakorn and Pinder, 1983).

Each equation in the system (A9) to (A11) represent N equations in N unknowns, which can be directly solved using Gaussian elimination. On boundaries of constant stream function and temperature, Ψ_n and T_n are known, therefore the equations of these nodes can be removed from the matrices. On boundaries of prescibed fluid and heat flow, q_n and J_n are inserted into the appropriate terms in the integrals. On the water-table surface, the hydraulic head is set equal to the elevation of the node, and the stream function condition is satisfied by setting B_n^Ω equal to the hydraulic head difference between the nodes on either side of node n on the boundary (Frind and Matanga, 1985). Note that in order to solve (A11) the Darcy velocity components must first be evaluated. Substituting the interpolation formula (A1) for hydraulic head into Darcy's law (1) yields:

$$q_x^e = -\sum_{j=1}^{3}\left[\frac{\mu_{rw}}{2\Delta}(K_{xx}b_jh_j)\right] \tag{A14}$$

$$q_z^e = -\sum_{j=1}^{3}\left[\frac{\mu_{rw}}{2\Delta}(K_{zz}c_jh_j) + K_{zz}\mu_{rw}\rho_{rw}\right] \tag{A15}$$

where the summation is over the three nodes in the element. Once the hydraulic heads are computed, the Darcy flux is calculated for each element with (A14) and (A15), and the results substituted into (A11). The fluid flow and heat transport equations are solved by updating pressure and temperature coefficients between time steps and iterating until the normalized temperature change between subsequent iterations is no greater than one percent at any node. Steady state models only require one set of iterations because time-stepping can be eliminated.

Numerical solutions of the oil mass transport equations, (7) and (8), are based on particle-tracking techniques and the stochastic theory of random walks (Bear, 1972). Source beds are represented by releasing several hundred mathematical particles. Each particle is assigned a mass, and they are assumed to move independently. The particles are tracked across the finite element grid with an algorithm that ensures they are also properly reflected at impermeable boundaries. During a time step, the p-th particle is advected according to the magnitude of the average linear velocity of the fluid in the element. New particle positions are computed in a simple fashion:

$$x_p^{k+1} = x_p^k + v_x \cdot \Delta t \qquad \text{(A16)}$$

$$z_p^{k+1} = z_p^k + v_z \cdot \Delta t \qquad \text{(A17)}$$

This time stepping process is repeated as necessary. For the case of soluble petroleum transport, particle positions after each advection step are modified with a random walk to simulate hydrodynamic dispersion in porous media. Random-walk displacements can be calculated from the root-mean-square distance of the particle ensemble and a uniform probability distribution (Ahlstrom and others, 1977). The dispersive steps are expressed as:

$$\Delta\tilde{x}_p = \sqrt{24 D_L \Delta t} \cdot (0.5 - \mathcal{R}) \qquad \text{(A18)}$$

$$\Delta\tilde{z}_p = \sqrt{24 D_T \Delta t} \cdot (0.5 - \mathcal{R}) \qquad \text{(A19)}$$

where $\Delta\tilde{x}$ and $\Delta\tilde{z}$ are the displacement along and transverse to the local fluid flow direction, D_L and D_T are the longitudinal and transverse dispersion coefficients, and R is a pseudo-random number in the range (0, 1). Concentrations are easily computed for each element in the mesh by enumerating the mass of particles in each element and dividing by the area. A major advantage of the particle-tracking method is that it does not experience problems of numerical dispersion or oscillation so common with finite element and finite difference techniques.

REFERENCES

Ahlstrom, S. W., Foote, H. P., Arnett, R. C., and Serne, R. J., 1977, Multicomponent mass transport model: Theory and numerical implementation: Richland, Washington, Batelle-PNL Report 2127, 114 p.

Anderson, W. G., 1987, Wettability literature survey—Part 5: The effects of wettability on relative permeability: Journal Petroleum Technology, November, p. 1453–1468.

Ball, M. W., 1935, Athabaska oil sands: Apparent example of local origin of oil: American Association Petroleum Geologists Bulletin, v. 19, p. 153–171.

Bally, A. W., Gordy, P. L., and Stewart, G. A., 1966, Structure, seismic data, and orogenic evolution of Southern Canadian Rocky Mountains: Canadian Petroleum Geology Bulletin, v. 14, p. 337–381.

Bear, J., 1972, Dynamics of Fluids in Porous Media: New York, Elsevier, 764 p.

Beaumont, C., 1981, Foreland basins: Royal Astronomical Society Geophysical Journal, v. 65, p. 291–329.

Beaumont, C., Boutilier, R., Mackenzie, A. S., and Rullkotter, J., 1985, Isomerization and aromatization of hydrocarbons and the paleothermometry and burial history of the Alberta foreland basin: American Association Petroleum Geologists Bulletin, v. 69, p. 546–566.

Bethke, C. M., 1985, A numerical model of compaction-driven groundwater flow and heat transfer and its application to the paleohydrology of intracratonic sedimentary basins: Journal Geophysical Research, v. 90B, p. 6817–6828.
———— 1986a, Hydrologic constraints on the genesis of the Upper Mississippi Valley district from Illinois basin brines: Economic Geology, v. 81, p. 233–249.
———— 1986b, Roles of sediment compaction, tectonic compression, and topographic relief in driving deep groundwater migration [abs.]: Geological Society America Abstracts with Programs, v. 18, p. 540.
Blanchard, P. E., and Sharp, J. M., 1985, Possible free convection in thick Gulf Coast sandstone sequence, *in* McNulty, C. L., and McPherson, J. G., eds., American Association Petroleum Geologists, Southwest Section, Fort Worth Geological Society, p. 6–12.
Bredehoeft, J. D., and Hanshaw, B. B., 1968, On the maintenance of anomalous fluid pressures, I. Thick sedimentary sequences: Geological Society America Bulletin, v. 79, p. 1097–1106.
Carrigy, M. A., 1974, Guide to the Athabasca oil sands area—introduction and general geology: Alberta Research Council Information Series 65, contribution 628, p. 3–13.
Cathles, L. M., and Smith, A. T., 1983, Thermal constraints on the formation of Mississippi Valley-type lead-zinc deposits and their implications for episodic basin dewatering and deposit genesis: Economic Geology, v. 78, p. 983–1002.
Cercone, K. R., ms, 1984, Diagenesis of Niagran (Middle Silurian) pinnacle reefs, northwest Michigan, Ph.D. dissertation, University of Michigan, Ann Arbor, 382 p.
Chamberlin, T. C., 1882, The ore deposits of southwestern Wisconsin: *in* Geology of Wisconsin: Wisconsin Geological Survey, v. 4, p. 365–571.
Clayton, J. L. and Swetland, P. J., 1980, Petroleum generation and migration in Denver Basin: American Association Petroleum Geologists Bulletin, v. 64, p. 1613–1633.
Corbett, C. S., 1955, In-situ origin of McMurray oil of northeastern Alberta and its relevance to general problem of origin of oil: American Association Petroleum Geologists Bulletin, v. 39, p. 1601–1649.
Cox, G. H., 1911, The origin of the lead and zinc ores of the Upper Mississippi Valley district: Economic Geology, v. 6, p. 427–448.
Dahlberg, E. C., 1982, Applied Hydrodynamics in Petroleum Exploration: New York, Springer-Verlag, 171 p.
Daubrée, A., 1887, Les Eaux Souterraines, aux Epoques Anciennes et a l'Epoque Actuelle: Paris, Dunod, 3 v.
Davis, R. W., 1987, Analysis of hydrodynamic factors in petroleum migration and entrapment: American Association Petroleum Geologists Bulletin, v. 71, p. 643–649.
Demaison, G. J., 1977, Tar sands and supergiant oil fields: American Association Petroleum Geologists Bulletin, v. 61, p. 1959–1961.
Deroo, G., Powell, T. G., Tissot, B., and McCrossan, R. G., 1977, The origin and migration of petroleum in the Western Canada sedimentary basin, Alberta: A geochemical and thermal maturation study: Geological Survey of Canada Bulletin 262, 136 p.
Dow, W. G., 1974, Application of oil-correlation and source-rock data to exploration in Williston Basin: American Association Petroleum Geologists Bulletin, v. 58, p. 1253–1262.
Dozy, J. J., 1970, A geologic model for the genesis of the lead-zinc ores of the Mississippi Valley, USA: Institute Mining and Metallurgy Transactions, Section B., v. 79, p. 163–170.
du Rouchet, J. H., 1981, Stress fields, a key to oil migration: American Association Petroleum Geologists Bulletin, v. 65, p. 74–85.
———— 1985, The origin and migration paths of hydrocarbons accumulated in the Lower Cretaceous sandstone "giant" tar accumulations of Alberta-II: Journal Petroleum Geology, v. 8, p. 101–114.
England, W. A., Mackenzie, A. S., Mann, D. M., Quigley, T. M., 1987, The movement and entrapment of petroleum fluids in the subsurface: Geological Society London Journal, v. 144, p. 327–347.
Eugster, H. P., 1985, Oil shales, evaporites, and ore deposits: Geochimica et Cosmochimica Acta, v. 49, p. 619–635.
Freeze, R. A., and Cherry, J. A., 1979, Groundwater: Englewood Cliffs, N.J., Prentice-Hall, 604 p.

Freeze, R. A., and Witherspoon, P. A., 1967, Theoretical analysis of regional groundwater flow: 2. Effect of water-table configurations and subsurface permeability variation: Water Resources Research, v. 3, p. 623–634.

Frind, E. O., and Matanga, G. B., 1985, The dual formulation of flow for contaminant transport modeling: 1. Review of theory and accuracy aspects: Water Resources Research, v. 21, p. 159–169.

Garven, G., 1985, The role of regional fluid flow in the genesis of the Pine Point deposit: Economic Geology, v. 80, p. 307–324.

——— 1986a, The role of regional fluid flow in the genesis of the Pine Point deposit—A reply: Economic Geology, v. 81, p. 1015–1020.

———1986b, A hydrogeologic model for the genesis of the giant oil sands deposits of the Western Canada sedimentary basin [abs.]: American Geophysical Union Transactions, v. 67, p. 273.

——— 1988, Effects of transient fluid flow on the thermal history of MVT mineralization [abs.]: Geological Society America Abstracts with Programs, v. 20, p. 364.

Garven, G., and Freeze, R. A., 1982, The role of regional groundwater flow in the formation of ore deposits in sedimentary basins: A quantitative analysis: Canadian National Hydrogeology Conference, Second Annual Meeting, Winnipeg, Manitoba, Proceedings, p. 60–67.

——— 1984a, Theoretical analysis of the role of groundwater flow in the genesis of stratabound ore deposits: 1. Mathematical and numerical model: American Journal of Science, v. 284, p. 1085–1124.

——— 1984b, Theoretical analysis of the role of groundwater flow in the genesis of stratabound ore deposits: 2. Quantitative results: American Journal of Science, v. 284, p. 1125–1174.

Ge, S., and Garven, G., 1988, Tectonically induced transient groundwater flow in sedimentary basins: American Geophysical Union Geodynamics Series (in press).

Gregg, J. M., 1985, Regional epigenetic dolomitization in the Bonneterre Dolomite (Cambrian), southeastern Missouri: Geology, v. 13, p. 503–506.

Gussow, W. C., 1956, Athabasca bituminous sands, *in* Symposium sobre yacimientos de petroleo y gas, v. 3: International Geological Congress, 20th, Mexico, Proceedings, p. 68–70.

Hacquebard, P. A., 1977, Rank of coal as an index of organic metamorphism for oil and gas in Albert, *in* G. Deroo, T. G. Powell, B. Tissot, and R. G. McCrossan, eds., The origin and migration of petroleum in the Western Canada sedimentary basin: Geological Survey of Canada Bulletin 262, p. 11–22.

Hearn, P. P., Jr., Sutter, J. F., and Belkin, H. E., 1987, Evidence of Late-Paleozoic brine migration in Cambrian carbonate rocks of the central and southern Appalachians: Implications for Mississippi Valley-type sulfide mineralization: Geochimica et Cosmochimica Acta, v. 51, p. 1323–1334.

Hitchon, B., 1969a, Fluid flow in the Western Canada sedimentary basin: 1. Effect of topography: Water Resources Research, v. 5, p. 186–195.

——— 1969b, Fluid flow in the Western Canada sedimentary basin: 2. Effect of Geology: Water Resources Research, v. 5, no. 2, p. 460–469.

——— 1974, Application of geochemistry to the search for crude oil and natural gas, *in* Levinson, A. A., ed., Introduction to Exploration Geochemistry: Calgary, Applied Pub., p. 509–545.

——— 1977, Geochemical links between oil fields and ore deposits, *in* Garrard, P., ed., Proceedings of the Forum on Oil and Ore in Sediments: London, Imperial College, p. 1–37.

——— 1984, Geothermal gradients, hydrodynamics, and hydrocarbon occurrences, Alberta, Canada: American Association Petroleum Geologists Bulletin, v. 68, p. 713–743.

Hitchon, B., and Filby, R. H., 1984, Use of trace elements for classification of crude oils into families—example from Alberta, Canada: American Association Petroleum Geologists Bulletin, v. 68, p. 838–849.

Hodgson, G. W., 1980, Origin of petroleum: In-transit conversion of organic compounds in water, *in* Roberts, W. H., III., and Cordell, R. J., eds., Problems of Petroleum Migration: American Association Petroleum Geologists, Studies in Geology 10, p. 169–178.

Hodgson, G. W., and Hitchon, B., 1965, Research trends in petroleum genesis: Edmonton, Alberta Research Council Contribution 270, 33 p.

Hoffmann, C. F., and Strausz, O. P., 1986, Bitumen accumulation in Grosmont platform complex, Upper Devonian, Alberta, Canada: American Association Petroleum Geologists Bulletin, v. 70, p. 1113–1128.
Hubbert, M. K., 1953, Entrapment of petroleum under hydrodynamic conditions: American Association Petroleum Geologists Bulletin, v. 37, p. 1954–2026.
Hume, G. S., 1947, Results and significance of drilling operations in the Athabasca bituminous sands: Canadian Institute Mining Metallurgy Engineering Transactions, v. 50, p. 298–324.
Hunt, J. M., 1977, Ratio of petroleum to water during primary migration in Western Canada basin: American Association Petroleum Geologists Bulletin, Geological Notes, v. 61, p. 434–435.
——— 1979, Petroleum Geochemistry and Geology: San Francisco, W. H. Freeman, 617 p.
Huyakorn, P. S., and Pinder, G. F., 1983, Computational Methods in Subsurface Flow: New York, Academic, 473 p.
Jackson, P. C., 1975, Geological Highway Map of Alberta: Geol. Highway Map Series: Calgary, Canadian Society Petroleum Geologists.
Jackson, S. A., and Beales, F. W., 1967, An aspect of sedimentary basin evolution: the concentration of Mississippi Valley-type ores during the late stages of diagenesis: Canadian Petroleum Geology Bulletin, v. 15, p. 383–433.
Jones, R. W., 1980, Some mass balance and geological constraints on migration mechanisms, *in* Roberts, W. H., III, and Cordell, R. J., eds., Problems of Petroleum Migration: American Association Petroleum Geologists, Studies in Geology 10, p. 47–68.
Jowett, E. G., 1986, Genesis of Kupferschiefer Cu-Ag deposits by convective flow of Rotliegende brines during Triassic rifting: Economic Geology, v. 81, p. 1823–1837.
Kaiser, C. J., Kelly, W. C., Wagner, R. J., and Shanks, W. C., III, 1987. Geologic and geochemical controls of mineralization in Southeast Missouri barite district: Economic Geology, v. 82, p. 719–734.
Kestin, J., Khalifa, H. E., and Correia, R. J., 1981, Tables of the dynamic and kinematic viscosity of aqueous NaCl solutions in the temperature range of 20–150°C and the pressure range of 0.1–35 MPa: Journal Physical Chemical Reference Data, v. 10, p. 71–87.
Kreyszig, E., 1972, Advanced Engineering Mathematics, 3d ed.: New York, John Wiley and Sons, 866 p.
Leach, D. L., and Rowan, E. L., 1986, Genetic link between Ouachita fold-belt tectonism and the Mississippi Valley-type lead-zinc deposits of the Ozarks: Geology, v. 14, p. 931–935.
Leenheer, M. J., 1983, Possible sources of Cretaceous oils and oil sands in the Western Canada basin: Conference on the Mesozoic of Middle North America Proceedings: Calgary, Canadian Society Petroleum Geologists, p. 55.
Levorsen, A. I., 1967, Geology of Petroleum, 2nd ed.: San Francisco, W. H. Freeman, 724 p.
Link, T. A., 1951, Source of oil in "Tar Sands" of Athabaska River, Alberta, Canada: American Association Petroleum Geologists Bulletin, v. 35, p. 854–864.
Margara, K., 1980, Agents for primary hydrocarbon migration: A review, *in* Roberts, W. H., III, and Cordell, R. J., eds., Problems of Petroleum Migration: American Association Petroleum Geologists, Studies in Geology 10, p. 33–45.
——— 1981, Mechanisms of natural fracturing in a sedimentary basin: American Association Petroleum Geologists Bulletin, v. 65, p. 123–132.
——— 1986, Geological Models of Petroleum Entrapment: London, Elsevier, 328 p.
Majorowicz, J. A., Rahman, M., Jones, F. W., and McMillan, N. J., 1985, The paleogeothermal and present thermal regimes of the Alberta basin and their significance for petroleum occurrences: Canadian Petroleum Geology Bulletin, v. 33, p. 12–21.
McAuliffe, C. D., 1980, Oil and gas migration: Chemical and physical constraints, *in* Roberts, W. H., III, and Cordell, R. J., eds., Problems of Petroleum Migration: American Association Petroleum Geologists, Studies in Geology 10, p. 89–107.
McCrossan, R. G., and Glaister, R. P., eds., 1964, Geological History of Western Canada: Calgary, Alberta Society of Petroleum Geologists, 232 p.
Moshier, S. O., and Waples, D. W., 1985, Quantitative evaluation of Lower Cretaceous Mannville Group as source rock for Alberta's oil sands: American Association Petroleum Geologists Bulletin, v. 69, p. 161–172.
Mossop, G. D., 1980, Geology of the Athabasca oil sands: Science, v. 207, p. 145–152.

Munn, M. J., 1909, The anticlinal and hydraulic theories of oil and gas accumulation: Economic Geology, v. 4, p. 509–529.

Neuzil, C. E., 1986, Groundwater flow in low-permeability environments: Water Resources Research, v. 22, p. 1163–1195.

Neuzil, C. E., and Pollock, D. W., 1983, Erosional unloading and fluid pressures in hydraulically tight rocks: Journal of Geology, v. 91, p. 179–193.

Noble, E. A., 1963, Formation of ore deposits by water of compaction: Economic Geology, v. 58, p. 1145–1156.

Nurkowski, J. R., 1984, Coal quality, coal rank variation and its relation to reconstructed overburden, Upper Cretaceous and Tertiary plains coals, Alberta, Canada: American Association Petroleum Geologists Bulletin, v. 68, p. 285–295.

Oliver, J., 1986, Fluids expelled tectonically from orogenic belts: Their role in hydrocarbon migration and other geologic phenomena: Geology, v. 14, p. 99–102.

Ozkaya, I., 1988, A simple analysis of primary oil migration through oil-propagated fractures: Marine and Petroleum Geology, v. 5, p. 170–174.

Palciauskas, V. V., and Domenico, P. A., 1980, Microfracture development in compacting sediments: Relation to hydrocarbon-maturation kinetics: American Association Petroleum Geologists Bulletin, v. 64, p. 927–937.

Peaceman, D. W., 1977, Fundamentals of Numerical Reservoir Simulation: Amsterdam, Elsevier, Developments Petroleum Science 6, 176 p.

Porter, J. W., Price, R. A., and McCrossan, R. G., 1982, The Western Canada sedimentary basin: Royal Society Philosophical Transactions, v. 305, p. 169–192.

Price, L. C., 1976, Aqueous solubility of petroleum as applied to its origin and primary migration: American Association Petroleum Geologists Bulletin, v. 60, p. 213–244.

Rich, J. L., 1921, Moving underground water as a primary cause and accumulation of oil and gas: Economic Geology, v. 16, p. 347–371.

——— 1931, Function of carrier beds in long-distance migration of oil: American Association Petroleum Geologists Bulletin, v. 15, p. 911–924.

Rabinowicz, M., Dandurand, J.-L., Jakubowski, M., Schott, J., and Cassan, J.-P., 1985, Convection in a North Sea oil reservoir: inferences on diagenesis and hydrocarbon migration: Earth and Planetary Science Letters, v. 74, p. 387–404.

Rubinstein, I., Strausz, O. P., Spyckerelle, C., Crawford, R. J., and Westlake, D. W. S., 1977, The origin of the oil sand bitumins of Alberta: A chemical and a microbiological simulation study: Geochimica et Cosmochimica Acta, v. 41, p. 1341–1353.

Sharp, J. M., Jr., 1978, Energy and momentum transport model of the Ouachita basin and its possible impact on formation of economic mineral deposits: Economic Geology, v. 73, p. 1057–1068.

Shi, Y., and Wang, C.-Y., 1985, High pore-pressure generation in sediments in front of the Barbados Ridge Complex: Geophysical Research Letters, v. 12, p. 773–776.

Shock, E. L., ms, 1987, Standard molal properties of ionic species and inorganic acids, dissolved gases and organic molecules in hydrothermal systems: Ph.D. dissertation, University of California, Berkeley, 260 p.

Siebenthal, C. E., 1915, Origin of the zinc and lead deposits of the Joplin region, Missouri, Kansas, and Oklahoma: U.S. Geological Survey Bulletin 606, 283 p.

Sproule, J. C., 1938, Origin of McMurray oil sands: American Association Petroleum Geologists Bulletin, v. 22, p. 1133–1152.

Stueber, A. M., Pushkar, P., and Hetherington, E. A., 1987, A strontium isotopic study of formation waters from the Illinois Basin, U.S.A.: Applied Geochemistry, v. 2, p. 477–494.

Streeter, V. L., and Wylie, E. B., 1975, Fluid Mechanics, 6th ed., : New York, McGraw-Hill, 752 p.

Sverjensky, D. A., 1986, Genesis of Mississippi Valley-type lead zinc deposits: Annual Reviews Earth and Planetary Science, v. 14, p. 177–199.

Thomas, G. E., 1962, Grouping of carbonate rocks into textural and porosity units for mapping purposes, *in* Ham, W. E., ed., Classification of Carbonate Rocks: American Association Petroleum Geologists Memoir 1, p. 193–223.

Tissot, B. P., and Welte, D. H., 1978, Petroleum Formation and Occurrence: Berlin, Springer-Verlag, 538 p.

Tóth, J., 1970, Relations between electric analogue patterns of groundwater flow and accumulation of hydrocarbons: Canadian Journal Earth Science, v. 7, p. 988–1007.
——— 1978, Gravity-induced cross-formational flow of formation fluids, Red Earth region, Alberta, Canada: Analysis, patterns, evolution: Water Resources Research, v. 14, p. 805–843.
——— 1980, Cross-formational gravity flow of groundwater: A mechanism of the transport and accumulation of petroleum (The Generalized Hydraulic Theory of Petroleum Migration), *in* Roberts, W. H., III., and Cordell, R. J., eds., Problems of Petroleum Migration: American Association Petroleum Geologists, Studies in Geology 10, p. 121–167.
Ungerer, P. Chénet, P. Y., Moretti, I., Chiarelli, A., and Oudin, J. L., 1985, Modeling oil formation and migration in the southern part of the Suez rift, Egypt: Organic Geochemistry, v. 10, p. 247–260.
van der Kamp, G., 1984, Evaluating the influence of groundwater flow systems on geothermal conditions, *in* Curtis, F. A., ed., Energy Developments, New Forms, Renewables, and Conservation: London, Pergamon Press, p. 297–301.
Van Hise, C. R., and Bain, H. F., 1902, Lead and zinc deposits of the Mississippi Valley, USA: American Institute Mining Engineering Transactions, v. 23, p. 376–434.
Vigrass, L. W., 1968, Geology of Canadian heavy oil sands: American Association Petroleum Geologists Bulletin, v. 52, p. 1984–1999.
Vugrinovich, R., 1988, Shale compaction in the Michigan Basin: Estimates of former depth of burial and implications for paleogeothermal gradients: Canadian Petroleum Geology Bulletin, v. 36, p. 1–8.
Welte, D. H., and Yukler, M. A., 1981, Petroleum origin and accumulation in basin evolution—A quantitative model: American Association Petroleum Geologists Bulletin, v. 65, p. 1387–1396.
Wood, J. R., and Hewett, T. A., 1984, Reservoir diagenesis and convective fluid flow: American Association Petroleum Geologists Memoir 37, p. 99–110.
Wright, G. N., ed., 1984, The Western Canada sedimentary basin—A series of geological sections illustrating basin stratigraphy and structure: Calgary, Canadian Society Petroleum Geologists and Geological Association of Canada.